New Vanadium, Titanium and Yttrium PNP Pincer Complexes based on 2,6-Diaminopyridine

Rita Alvarez Ruivo

Thesis to obtain the Master of Science Degree in

Chemical Engineering

Supervisor: Prof. Dr. Ana Margarida Sousa Dias Martins

Examination Committee

Chairperson: Prof. Dr. Carlos Manuel Faria de Barros Henriques

Supervisor: Prof. Dr. Ana Margarida Sousa Dias Martins

Members of the Committee: Dr. Sónia Duarte. Barroso

October 2016

THIS PAGE LEFT BLANK INTENTIONALLY

Acknowledgements

First, I would like to thank Prof. Ana Margarida Martins for being my supervisor, giving me the opportunity to work in her amazing research group. I would also like to thank Prof. Karl Kirchner for receiving me kindly in his research group and for sharing his knowledge about pincer chemistry.

Thank you Sara for receiving me in Vienna, for taking care of me and for helping me every time I needed.

Thank you Luís, for all the support inside and outside the laboratory. Although not my supervisor, you guided me through this work.

Many thanks to all my colleagues, Ana, Adhan, Clara, Cláudia, Luís, Filipe, Patrícia, Sónia and Tiago for providing me all the laughs and cheers.

To Miguel, thank you for your never-ending optimism and assistance. A special thank you to my mother and to my grandfather for the endless support and encouragement. Without any of you this wouldn't be possible.

Finally, I would like to dedicate this work to my beloved grandmother. I'm always and forever thankful for growing next to you.

Abstract

The synthesis of early transition metal complexes based on 2,6-diaminopyridine PNP ligands is reported. Vanadium complexes of the formula [V(PNP-$^{i}Pr_2$)Cl_3], [V(PNP-Ph_2)Cl_3], [V(PNP^{Me}-$^{i}Pr_2$)Cl_3] and the titanium complex [Ti(PNP-Ph_2)Cl_3] were characterized by infrared spectroscopy, elemental analysis and X-ray crystallography. The complex [V(PNP-Ph_2)Cl_3] was also prepared, in the absence of solvent, through mechanochemistry. The yttrium complex [Y(PNP)Cl_2][YCl_4] was characterized by infrared spectroscopy, elemental analysis and ESI-MS. Titanium and yttrium PNP pincer complexes are described here for the first time. In a preliminary reactivity study, the vanadium complexes showed unpredictable behaviour related to the strong acidity of the metal center and to the presence of a non-innocent NH spacer.

Keywords: Vanadium complexes; Titanium complexes; Yttrium complexes; Pincer ligands

Resumo

Neste trabalho apresenta-se a síntese de complexos metálicos da esquerda da tabela periódica (vanádio, titânio e ítrio) suportados por ligandos PNP derivados de 2,6-diaminopiridina. Os complexos de vanádio com a fórmula [V(PNP-^{i}PR$_2$)Cl$_3$], [V(PNP-Ph$_2$)Cl$_3$], [V(PNP^{Me}-^{i}PR$_2$)Cl$_3$] e um complexo de titânio do tipo [Ti(PNP-Ph$_2$)Cl$_3$] foram caracterizados por espectroscopia de infravermelho, análise elementar e cristalografia de raios-X. O complexo [V(PNP-Ph$_2$)Cl$_3$] foi também preparado por mecanoquímica, na ausência de solvente. O complexo de ítrio [Y(PNP)Cl$_2$][YCl$_4$] foi caracterizado por espectroscopia de infravermelhos, análise elementar e ESI-MS. Os complexos pincer PNP de vanádio e ítrio são descritos aqui pela primeira vez. O estudo preliminar de reactividade dos complexos de vanádio demonstrou um comportamento imprevisível que pode estar associado à forte acidez do centro metálico e à presença de um espaçador NH não-inocente.

Palavras-Chave: Complexos de vanádio; Complexos de titânio; Complexos de ítrio; Ligandos pincer.

Table of Contents

List of Tables

List of Figures

Abbreviations and Symbols

BIPOL	dibenzo[d,f][1,3,2]dioxaphosphepine
EA	Elemental Analysis
Equiv.	equivalent
ESI	Electrospray Ionization
Et	ethyl
Et_2O	diethylether
FIR	Far Infrared Radiation
FT/IR	Fourier Transform Infrared
Me	methyl
MeCN	acetonitrile
MS	Mass Spectrometry
MW	Molecular Weight
Net_3	Triethylamine
NMR	Nuclear Magnetic Resonance
nPr	propyl
ppm	parts per million
Ph	phenyl
^{i}Pr	isopropyl
^{t}Bu	Tert-butyl
THF	tetrahydrofurane
δ	Chemical shift
Δ	heat

Introduction

The first organometallic compound, $K[PtCl_3(CH_2=CH_2)]$, prepared by Zeise in 1827 awoke the world to organometallic chemistry, though it was only in the 1950's with the synthesis of ferrocene that organometallic chemistry really boomed and developed into a major discipline. [1]

The premise for this branch of chemistry is that association of a metal centre and an organic fragment profoundly modifies the properties of both single components, such as solubility and reactivity, having also a strong influence on selectivity. This effect is intimately related to the properties of the ancillary ligands that hold the metal centre and thus, the design of new ligands is one of the main goals in organometallic chemistry and catalysis.

The first reports on transition metal pincer complexes were published in the late 1970s and early 1980s. [2] Since then, there has been a blooming interest in such complexes due to their characteristics and properties, such as their robust nature, extraordinary thermal stability, accessibility of synthetic methods and the spectacular chemical transformations that they can mediate. [3] Due to the ability of fine tuning the steric and electronic properties of the pincer ligands, which, in turn change the physical and electronic properties, and hence, the reactivity of the complexes, such species are continuously investigated for various applications in homogenous catalysis. [3, 4]

Pincer ligands are tridentate species that bind tightly to three coplanar coordination sites of a transition metal, mostly in a meridional configuration. The form EXE can describe this type of chelating agents where X is the central, anchoring Lewis donor (Lewis base) and E are two flanking Lewis donors (see Figure 1).

Pincer ligands are named according to the donor atoms. Functional groups and spacers can also be referred, as exemplified by the PNP^{Me}-Ph terminology used in this work, which describes a diphosphine/pyridine pincer donor with a methylamine spacer and two phenyl groups on the phosphine moieties.

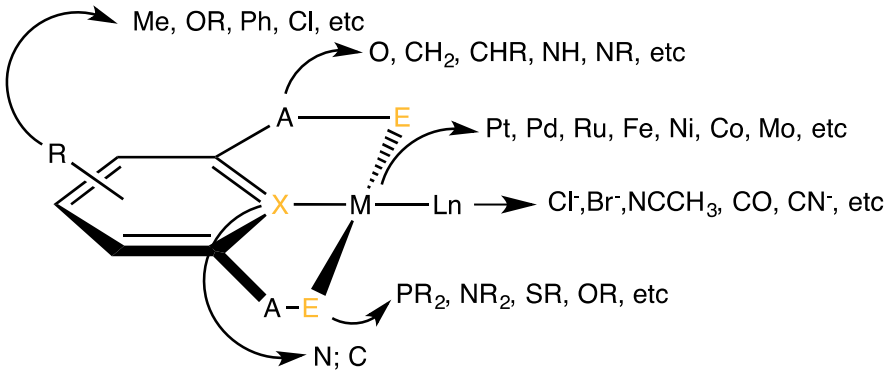

Figure 1 – General representation of pincer complexes.

As already mentioned, pincer ligands offer the possibility of building different ligand architectures by changing the anchoring flanking donors or the linkers, in flexible and diverse approaches. A wide range of pincer ligands, such as PCP, SCS, NCN and much more EXE combinations has thus been reported in the literature. Among them, anionic PCP ligands based on 1,3-disubsituted benzenes were the first to be described and still represent the most widely used pincer structures. [5]

MX_2 precursors of group 10 (M=Ni, Pd, Pt) and MX_3 of group 9 (M=Rh, Ir) (X=Cl) were used for the synthesis of the first PCP complexes reported by Shaw *et al.* [3] The bonding of soft ligands ($E=PR_2$, SR_2) to d^8 transition metals is highly favoured and the formation of the M-C bonds generally takes place via activation of the C_{sp2}-H or C_{sp3}-H bonding, thereby generating an acid molecule of HX. [6]

Pincer complexes have been employed in various stoichiometric bond activation reactions and catalytic processes involving oxidative addition reactions and coupling processes such as the Heck reaction, Suzuki-Miyaura coupling, dehydrogenation of alkanes, asymmetric allylic alkylation, hydrogen transfer reactions as well as other relevant applications (see Figure 2). [7, 8, 9 , 10, 11, 12]

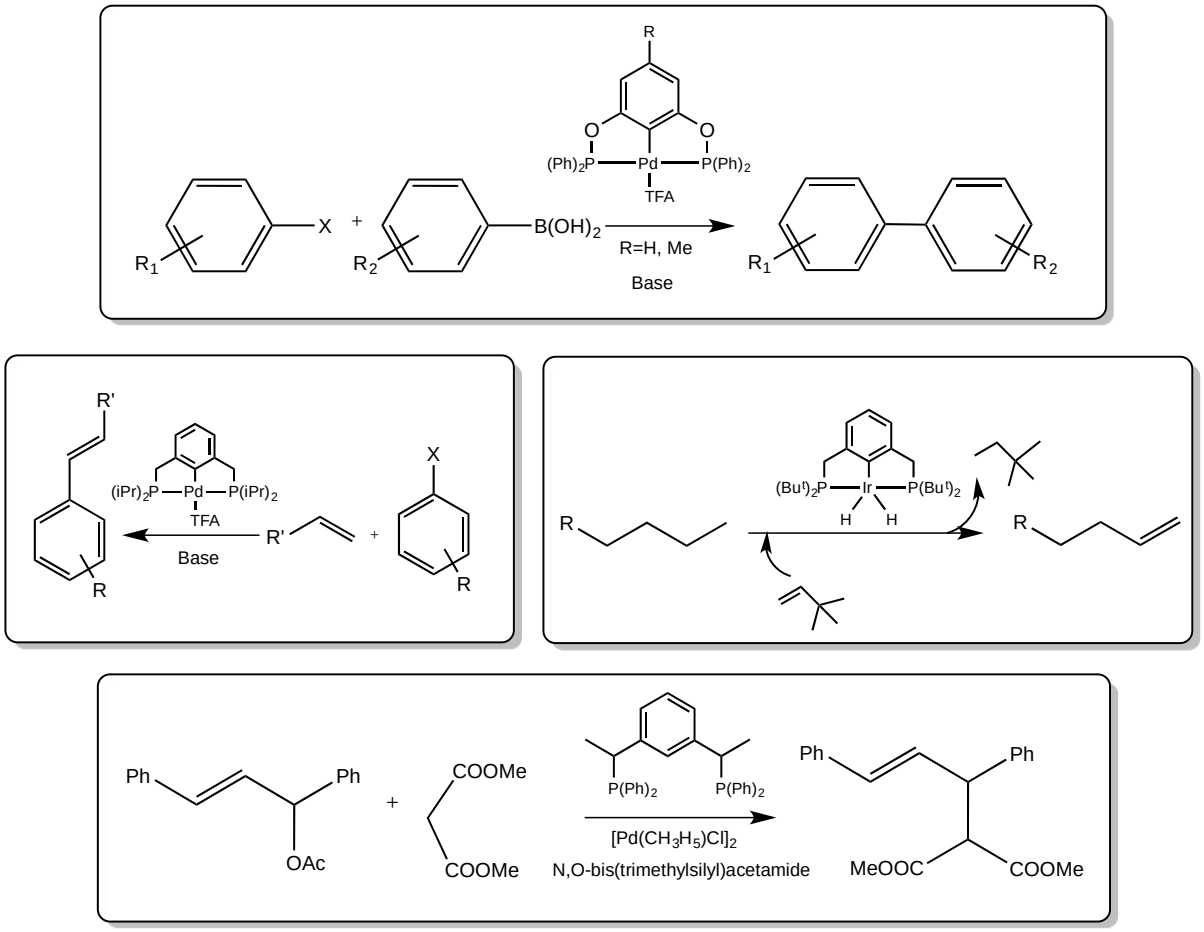

Figure 2 – Clockwise (top to bottom): Suzuki-Miyaura coupling with a Pd^{II}-PCP complex; Heck reaction using a Pd^{II}-PCP catalyst and dehydrogenation of alkanes with an Ir^{II} catalyst; Asymmetric allylic alkylation by $[Pd(C_3H_5)Cl_2]_2$. [13, 14, 15, 16]

Haupt *et al.* came across a new family of amino-bridged PNP pincer ligands resulting from the reaction of 2,6-diaminopyridine with chlorophosphines. [17] This class of nitrogen-based ligands provides a hybrid environment that combines soft phosphines and a hard amine donor, and it is likely that such ligands are suitable to support both hard early transition metal centres and soft late transition metal centres. PNP ligands in which the central pyridine-based ring donor contains $-CH_2PR_2$ substituents in the two *ortho* positions are widely used in transition metal chemistry. Yet, although these ligands can be manipulated to control the reactivity at metal centers, they have two major drawbacks: their stereochemical parameters are difficult to modify, often requiring several multistep synthesis, and the organic precursors are not commercially available or are expensive. With regard to these disadvantages, the PNP ligands used in

this work, having –$NHPR_2$ linkers instead of carbon-based moieties, are readily prepared and provide a direct method for obtaining varied steric, electronic and stereochemical ligand properties. [2]

Milstein and co-workers discovered highly efficient pyridine-based PNP ruthenium complexes that catalyse the hydrogenation of ketones to alcohols and the hydrogenation of CO_2 to formate salts, where the central pyridine backbone is connected to –CH_2PR_2 and/or CH_2NR_2 substituents.[18] Hydrogenation of ketones and amides catalysed by transition metal complexes is a fundamental process for the production of a wide range of alcohols and amines. Although the most effective catalysts are based on PCP ligands, PNP complexes are also efficient hydrogenation catalysts, as pointed out by the recent study of iron complexes of the type [Fe(PNP-$^{i}Pr_2$)(H)(BH_4)(CO)], [Fe(PNP-$^{t}Bu_2$)$(H)_2$(CO)] and [Fe(PNP-$^{i}Pr_2$)(H)(Br)(CO)]. [18] For these compounds, the splitting of a coordinated highly acidic H_2 molecule occurs through a heterolytic process, such that the proton is accepted by an external or internal Lewis base while leaving the hydride on the metal center.

Kirchner and co-workers[19] showed that the reaction of [Fe(PNP-$BIPOL_2$)$(CH_3CN)_3]^{2+}$ with an excess of NaHg resulted in an immediate evolution of H_2, affording the deprotonated, dearomatized, monocationic complex, represented in Figure 3. The authors stated that the deprotonation is reversible, and addition of HBF_4 to a solution of [Fe(PNP-$BIPOL_2$)$(CH_3CN)_3]^{+}$ cleanly afforded the dicationic complex where the pydirine ring regained aromaticity.

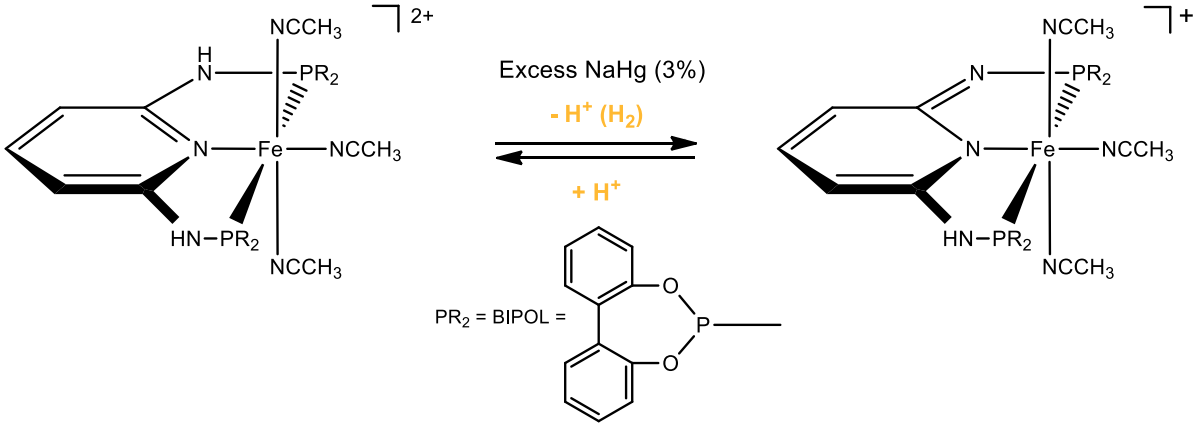

Figure 3 – Formation of [Fe(PNP-$BIPOL_2$)$(CH_3CN)_3]^{+}$ complex through metal-ligand cooperation. Adapted from [19].

A non-innocent ligand behavior was also noticed in the formation of the Fe(II) complex *cis*-[Fe(PNP-^{i}Pr$_2$)(CO)$_2$H]$^+$ displayed in Figure 4. Once again it is proposed that the heterolytic hydrogen cleavage involves the reversible dearomatization and rearomatization of the pyridine fragment.

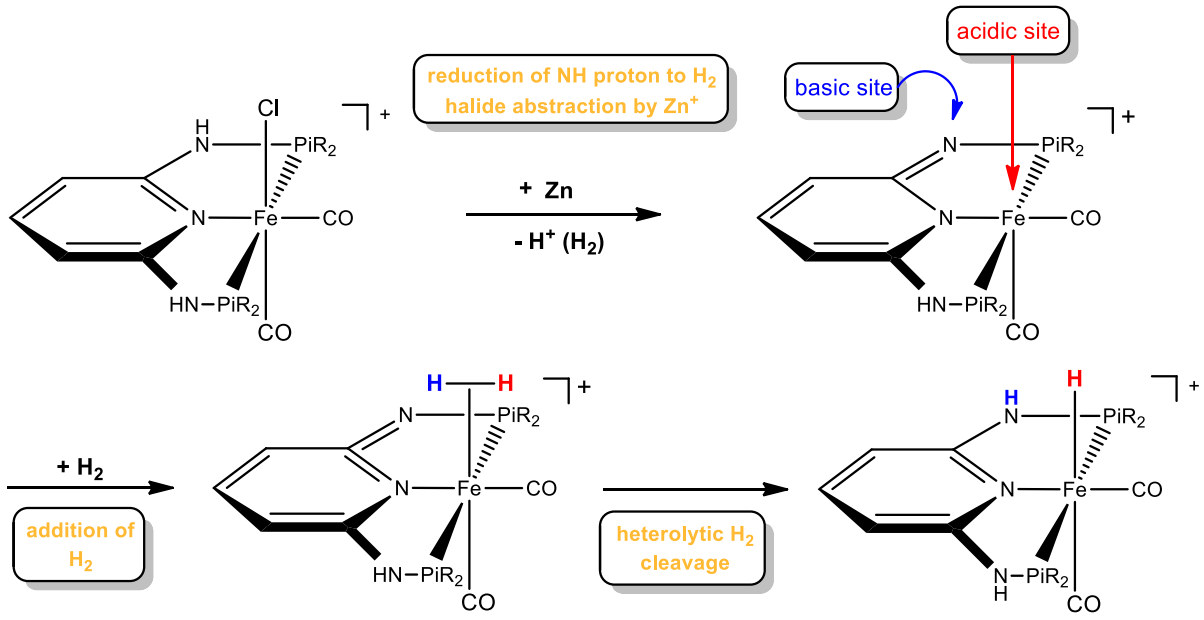

Figure 4 – Formation of *cis*-[Fe(PNP-^{i}Pr$_2$)(CO)$_2$H]$^+$ complex by heterolytic hydrogen cleavage involving the dearomatization of the ligand. Adapted from [19].

The same reaction was attempted with the related complex *trans*-[Fe(PNP^{Me}-^{i}Pr$_2$)(CO)$_2$Cl]$^+$ and, as anticipated, due to the lack of acidic protons for the metal-ligand cooperation, the N-methylated complex did not react with Zn.

Kirchner and co-workers also reported that PNP ligands sterically less demanding than PNP-^{i}Pr$_2$, lead to complexes of the type [Fe(k^3-P,N,P-PNP)(k^2-P,N-PNP)X]$^+$ (X=Cl, Br) (independently of whether 1 or 2 equiv. of ligands are used) while penta-coordinate complexes [Fe(k^3-P,N,P-PNP)X^2] are obtained with bulkier ligands (see Figure 5). [20, 21]

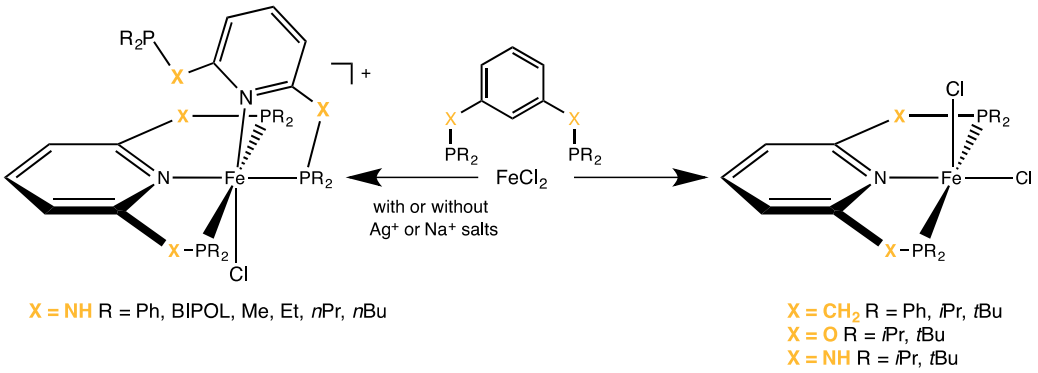

Figure 5 – Reactivity differences for the formation of Fe complexes between several PNP ligands.

In an attempt to prevent the coordination of a second PNP ligand, the N-methylated and N-phenylated ligands (PNP^{Me}-Ph_2, PNP^{Ph}-Et_2 and PNP^{Ph}-nPr_2) were employed in the reaction described in Figure 5. The second ligand coordination did not occur for N-phenylated ligands. On the other hand, the reaction of $FeCl_2$ with 2 equiv. of PNP^{Me}-Ph_2 is accompanied by P-N bond cleavage, yielding the cationic complex $[Fe(k^3\text{-}P,N,P\text{-}PNP^{Me}\text{-}Ph)(k^2\text{-}P,N\text{-}PNH^{Me}\text{-}Ph)Cl]^+$. Despite the ubiquitous presence of phosphines in pincer chemistry, phosphine degradation (and thus PNP ligands) may constitute a problem. The P-N bond can be readily cleaved by hydrolysis, under acidic or strongly basic conditions in the presence of water, as shown in Figure 6, forming for instance Ph_2POH.

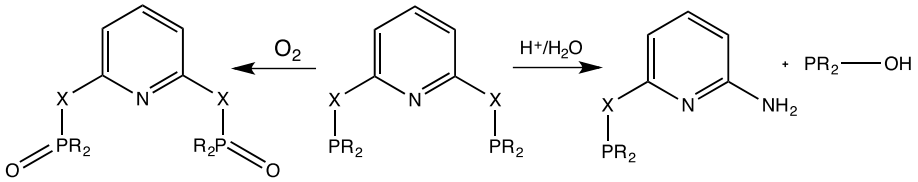

Figure 6 – P-N bond cleavage.

Neutral tridentate systems such as PNP have emerged as leading platforms for the study of catalytic reactions, but a brief survey of the literature indicates that research has mainly dealt with complexes containing precious metals such as ruthenium, iridium and palladium.

Given the high cost of those metals a number of reports have appeared in which such base-metal complexes were deployed in fields ranging from energy to catalysis. [22]

Other PNP complexes of transition metals such as molybdenum, nickel, iron, cobalt have started being explored but titanium, yttrium and vanadium pincer complexes remain unknown so far, as indicated in Figure 7.

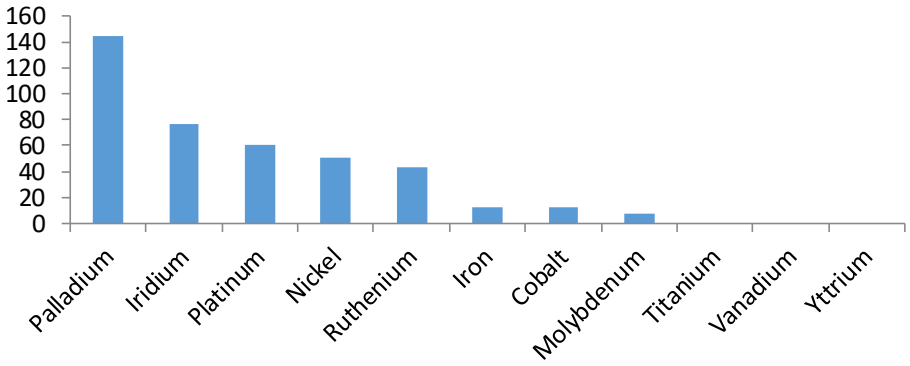

Figure 7 – Search results for 'pincer (metal)' in ScienceDirect, as of 20/05/2016.

The increasing interest in pincer complexes, allied with the scarcity and the high prices of precious metals makes desirable the use of more sustainable metals such as nickel, cobalt, molybdenum and iron, which recently started to be explored.

This work is a preliminary contribution to the study of new pincer complexes of transition metals such as vanadium, titanium and yttrium, which have not yet been reported.

Results and Discussion

Synthesis and Characterization of Pincer Complexes

PNP-$^{i}Pr_2$ **1** and PNP-Ph_2 **2** were prepared in toluene at 80°C by a one-pot reaction using the suitable chlorophosphine and 2,6-diaminopyridine in the presence of NEt_3 (see Scheme 1).[4] This reaction proceeds through a nucleophilic attack of the amine on the phosphorous, with the formation of NEt_3·HCl that precipitates out of solution.

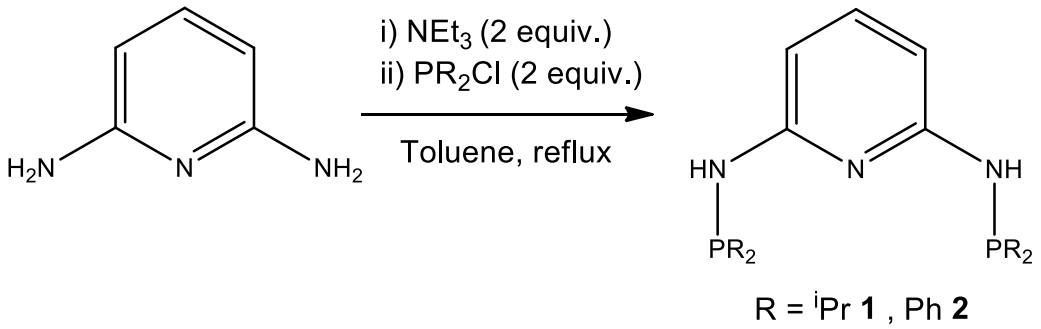

Scheme 1 – Synthesis of the organic PNP precursors, PNP-$^{i}Pr_2$ and PNP-Ph_2.

The progress of the reactions was checked by ^{1}H NMR and ^{31}P NMR. As the reaction occurs, the ^{31}P signals of the ligands start being visible at δ [PNP-$^{i}Pr_2$] = 48.4 ppm and δ [PNP-Ph_2] = 24.6ppm, which represent high field shifts, in comparison with the corresponding chlorphosphines signals at δ [$^{i}Pr_2PCl$] = 134 ppm and δ [Ph_2PCl] = 81.5 ppm. Both compounds **1** and **2** were obtained at 81% yield after flash chromatography.

The ^{1}H NMR spectrum of PNP-$^{i}Pr_2$ shows characteristic resonances of the pyridine protons at δ=7.23 and δ=6.42 ppm that integrate 1:2 and correspond to the H_{para} and to H_{meta}, respectively. In the proton NMR spectrum of PNP-Ph_2, only the resonance assigned to H_{meta} of the pyridine moiety is observed at δ=6.53 ppm, due to the overlap with the phenyl ring resonances.

The resonances of the amino protons appear at δ=4.48 ppm for the PNP-$^{i}Pr_2$ and at δ=5.47 for PNP-Ph_2. The ^{1}H NMR spectrum of PNP-$^{i}Pr_2$ also reveals two multiplets at δ=1.72 and δ=1.07-0.97 ppm corresponding to the CH and CH_3 groups of the isopropyl substituents, respectively. The ^{1}H NMR spectrum of PNP-Ph_2 shows a multiplet in the aromatic region at δ=7.46-7.36 ppm corresponding to the protons of the phenyl groups.

In the infrared spectrum, representative resonances of **1** and **2** bonds are found. The characteristic frequencies for the ring stretching of 2-substituted pyridine are showed in the region of 1615 to 1433 cm^{-1}. More specifically, the C-N bond in primary aromatic amines with the nitrogen directly on the ring absorbs strongly at 1330 to 1260 cm^{-1}. The P-NH group absorbs at 3200 to 2900 cm^{-1}, while the N-H group of the amine spacer absorbs at 3500 to 3400 cm^{-1}, 1650 to 1550 and at 750 to 700 cm^{-1}. In compound **1** the CH_3 asymmetrical deformation of the isopropyl groups of the phosphines can be found in the region of 2970 to 2850 cm^{-1} and at 1420 cm^{-1}. The phenyl group attached to the phosphorous in compound **2** may give rise to the following bands: 3050 cm^{-1}, 1600 cm^{-1} to 1500 cm^{-1}, 1450 to 1425 cm^{-1}, 1130 to 1090 cm^{-1}, 1010-990 cm^{-1}, 750 cm^{-1} and 700 cm^{-1} .[23]

From the analysis of the various infrared characteristic frequencies of compounds **1** and **2**, the overlay of representative bands makes singular identification difficult, as observed in Figure 8 and 9. However, in both spectra it is possible to identify in the region from 3400 to 2800 cm^{-1} bands belonging to the P-N bond, the amine spacer and the isopropyl and phenyl groups, in **1** and **2**, respectively.

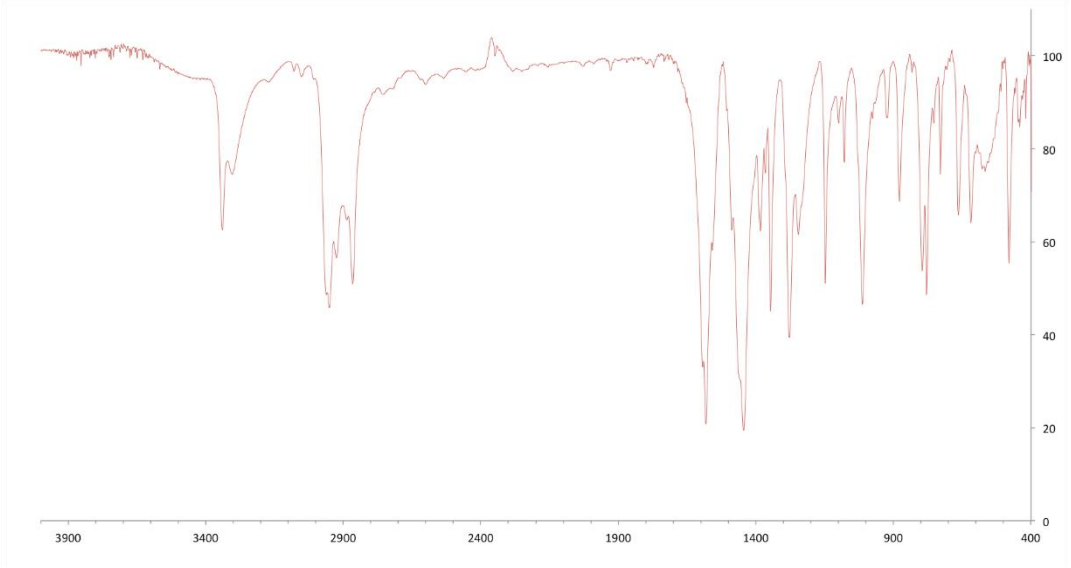

Figure 8 – Infrared Spectrum of PNP-$^{i}Pr_2$.

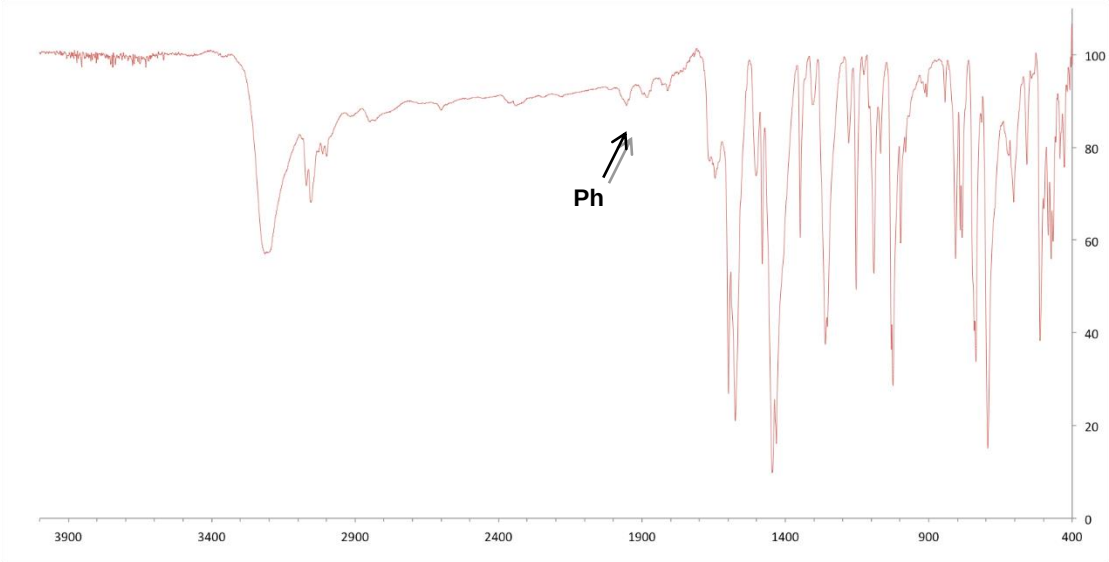

Figure 9 - Infrared Spectrum of PNP-Ph_2.

The characteristic pattern of mono substituted benzenes belonging to **2** can be found in the three bands at 1953, 1881 and 1804 cm^{-1}.

In both spectra the region of 1700 to 400 cm^{-1} displays several bands belonging to overlapped frequencies of the pyridine backbone, the amine spacer and the isopropyl and phenyl groups, in **1** and **2**, respectively.

Using ligands **1** and **2** and $(THF)_3VCl_3$ as the vanadium precursor, complexes $[V(PNP\text{-}^iPr_2)Cl_3]$ **3** and $[V(PNP\text{-}Ph_2)Cl_3]$ **4** were synthesized (see Scheme 2).

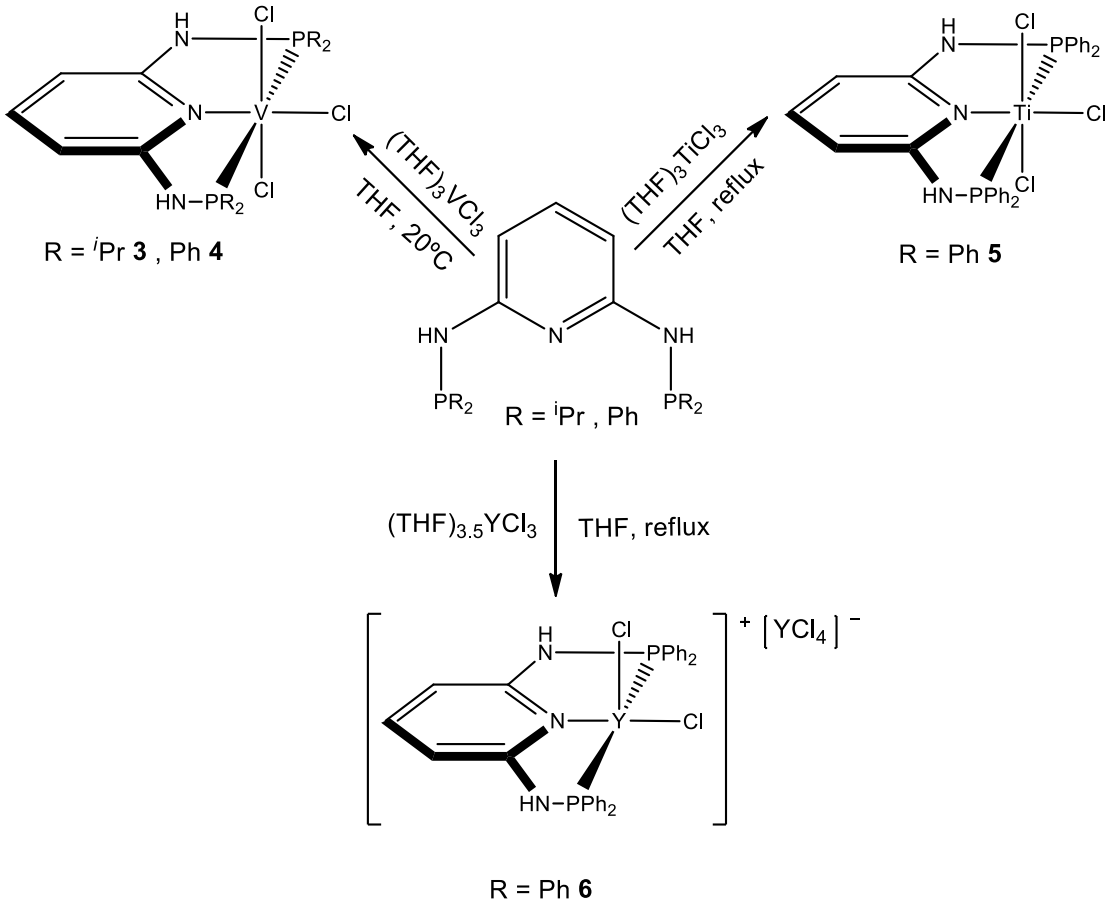

Scheme 2 – Synthesis of vanadium, titanium and yttrium PNP complexes.

Reactions of $(THF)_3VCl_3$ in THF with PNP-PR_2 solutions (R = $^iPr_2$, Ph_2) in the same solvent led to a green solution with a brown precipitate for R = $^iPr_2$ and to a brown solution with a green precipitate for R = Ph_2. For the first reaction, elemental analysis of both the precipitate and the product that was initially in solution gave the same result. Thus, $[V(PNP\text{-}^iPr_2)Cl_3]$ **3** may be obtained as a brown solid by evaporation of the solvent of the reaction mixture under vacuum without removal of the precipitate. However in the reaction of $(THF)_3VCl_3$ with PNP-Ph_2 only the green precipitate corresponds to $[V(PNP\text{-}Ph_2)Cl_3]$ **4**. The complexes were obtained in moderate yields, of 72% and 60%, for **3** and **4**, respectively.

Complex **4** was also prepared by a solid state reaction using mechanosynthesis. A mixture of $(THF)_3VCl_3$ and PNP-Ph_2 in the molar ratio of 1:1.1 was placed in an acrylic

glass reaction vessel and milled for 10 minutes, after which the colour of the mixture changed from pink to dark green. The reaction product was washed with toluene and upon drying, was subjected to elemental analysis, revealing a mixture of $(THF)_3VCl_3$ and **4** in the ratio 2:1. This result indicates that mechanosynthesis is an appropriate method for the synthesis although longer reaction times are necessary to complete the reaction. This preliminary result was not further explored but it certainly deserves being continued.

Complexes $[V(PNP\text{-}^{i}Pr_2)Cl_3]$ **3** and $[V(PNP\text{-}Ph_2)Cl_3]$ **4** were characterized by IR spectroscopy as depicted in Figure 10 and Figure 11, respectively. In terms of spectral regions, it is possible to find bands in the region from 3400 to 2800 cm^{-1} belonging to the P-N bond, the amine spacer and the isopropyl and phenyl groups of **3** and **4**.

The characteristic pattern bands of mono substituted benzenes belonging to **4** can be found in the three bands at 1964, 1891 and 1815 cm^{-1}.

In both complexes **3** and **4** the region of 1700 to 400 cm^{-1} displays several bands belonging to overlapped frequencies of the pyridine backbone, the amine spacer and the isopropyl and phenyl groups, in **3** and **4**, respectively.

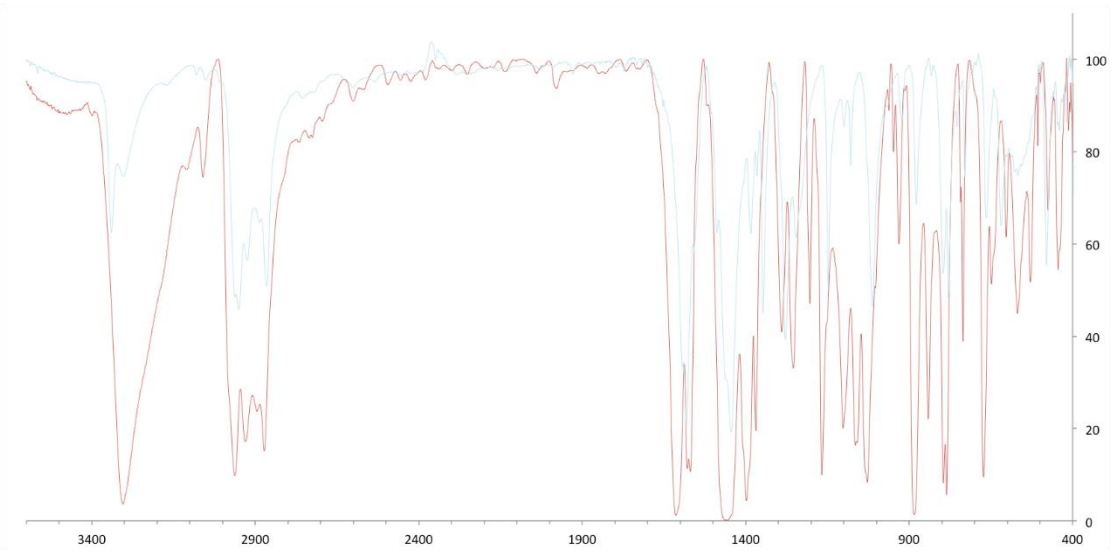

Figure 10 – Infrared spectra overlap between $[V(PNP\text{-}^{i}Pr_2)Cl_3]$ (in red) and the respective ligand (in blue).

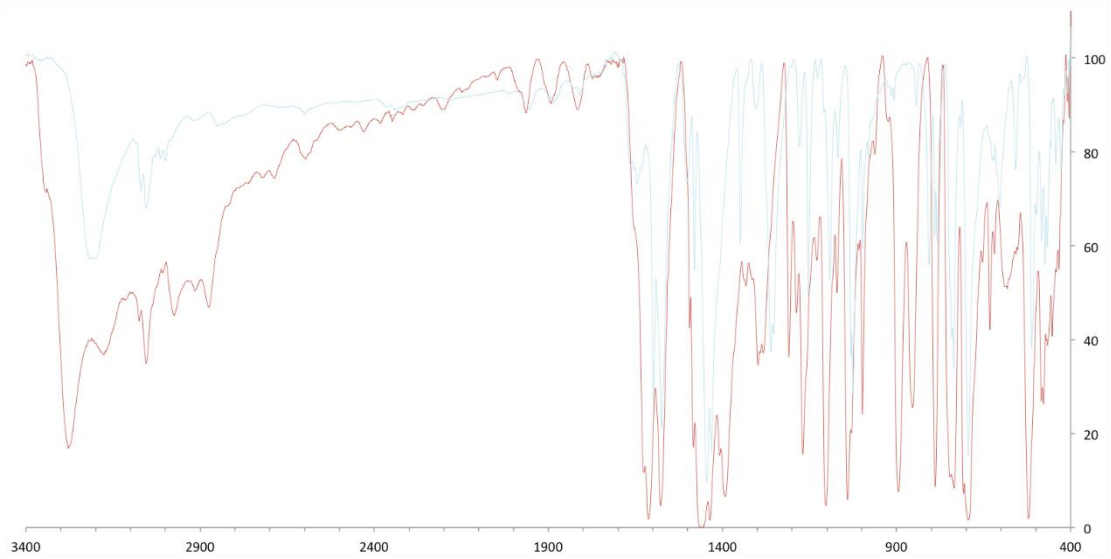

Figure 11 - Infrared spectra overlap between [V(PNP-Ph_2)Cl_3] (in red) and the respective ligand (in blue).

When compared with the ligands **1** and **2**, the spectral regions in both complexes were moved to high frequencies and the signals became more intense. The number of bands was also increased which can be due to the metal coordination and thus the loss of symmetry.

Moreover, complexes **3** and **4** were investigated by means of ESI-MS. In the negative mode, the most abundant signals are observed at m/z equal to 534.11 **3** and 669.33 for **4** which correspond to the anionic complexes [V(PNP-PR_2)Cl_4]$^-$. Signals at m/z of 498.13 **3** and 632.18 **4** correspond to the starting complexes with loss of a proton in the amino spacer [V(PNP-PR_2)Cl_3]$^-$. In the positive mode, the most intense signals for complex **3** are noticed at m/z equal to 443.38 and 462.20 which correspond to [V(PNP-^{i}Pr$_2$)ClO]$^+$ and [V(PNP-^{i}Pr$_2$)Cl_2]$^+$, respectively. For complex **4**, signals at m/z of 707.85 and 597.12 are consistent with the complexes [V(PNP-Ph_2)Cl_2(2.6-diaminopyridine)]$^+$ and [V(PNP-Ph_2)ClO]$^+$.

The bonding of a diaminopyridine fragment to complex **4** identified by ESI-MS is not surprising. As stated by Kirchner and co-workers[20, 21], iron PNP-Ph_2 complexes with the –NH spacer undergo facile rearrangement reactions to give cationic complexes of the type [Fe(κ^3-P,N,P-PNP-Ph)(κ^2-P,N-PNP-Ph)Cl]$^+$ while ligands more sterically demanding, such has PNP-^{i}Pr$_2$ originate complexes of the type [Fe(k^3-P,N,P-PNP)Cl_2].

Although the result from ESI-MS reveals the formation of **4** bearing only the diaminopyridine fraction from the ligand, it is plausible that the ionization produced by this technique resulted in the fragmentation of the complex $[V(PNP\text{-}Ph_2)Cl_2(PNP)]^+$.

The paramagnetic susceptibility of the vanadium complexes **3** and **4** was measured using Evan's method (see Table 1). [24, 25, 26, 27]

Table I - Effective magnetic number for complexes 3 and 4.

$\mu_{eff,obs}$	Hours after contact with air	
	0	2
(3) $[V(PNP\text{-}^iPr_2)Cl_3]$	2.84	2.31
(4) $[V(PNP\text{-}Ph_2)Cl_3]$	2.56	2.35

For both complexes **3** and **4**, the values obtained for $\mu_{eff,obs}$ are well compared with the theoretical effective magnetic number $\mu_{eff} = 2.83$. This value was calculated for a d^2 metal centre of $2e^-$ through $\mu_{eff} = \sqrt{n(n+2)}$, where n is the number of unpaired electrons.

As displayed in Table 1, the experimental values obtained immediately after the preparation of the samples, are very close to the theoretical value. However, the values obtained after 2 hours in contact with air are smaller, suggesting that partial oxidation took place evidencing that the complexes are not stable in solution in the presence of air.

A cyclic voltammetry study of $[V(PNP\text{-}^iPr_2)Cl_3]$ **3** in THF and dichloromethane in the presence of nitrogen was carried out. The results are displayed in Figure 12.

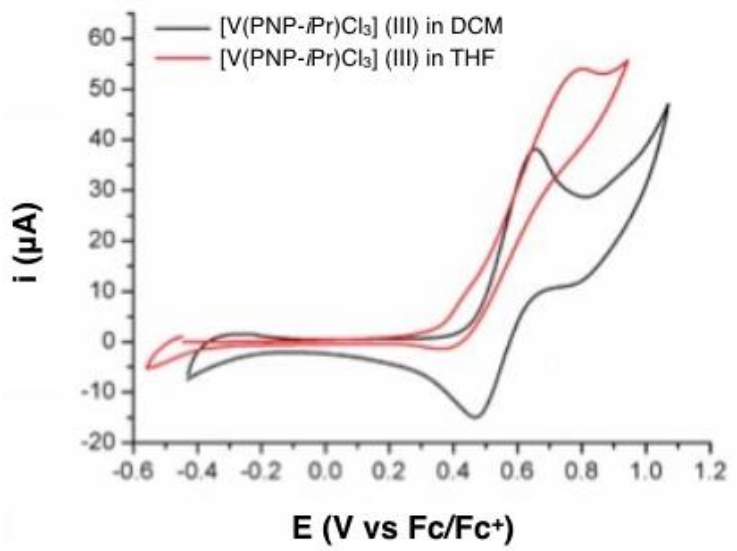

Figure 12 - Cyclic voltammograms of 3 in CH_2Cl_2 and THF.

In dichloromethane a quasi-reversible V^{III}/V^{IV} couple is observed, with an oxidation process at 0.65 V and its corresponding reduction at 0.47 V, suggesting that the cation $[V(PNP\text{-}^{i}Pr_2)Cl_3]^+$ is relatively stable in CH_2Cl_2 solution. However, in THF an irreversible oxidation of the V^{III} complex is observed. The irreversible nature of the oxidation process is likely associated to the donor properties of THF, which may induce a chemical process that takes place after oxidation. At present it is not possible to identify the decomposition process that takes place, although formation of oxovanadium from reaction with residual oxygen or water may not be excluded. [28]

The solution of **3** in CH_2Cl_2 used in this study was held in contact with air for several days, and the cyclic voltammograms were repeated throughout this time. The results, showed in Figure 13 reveal that the oxidation product initially formed in Figure 12 is not stable in the presence of air, changing from an initially brown solution to a blue solution at the end of the third day.

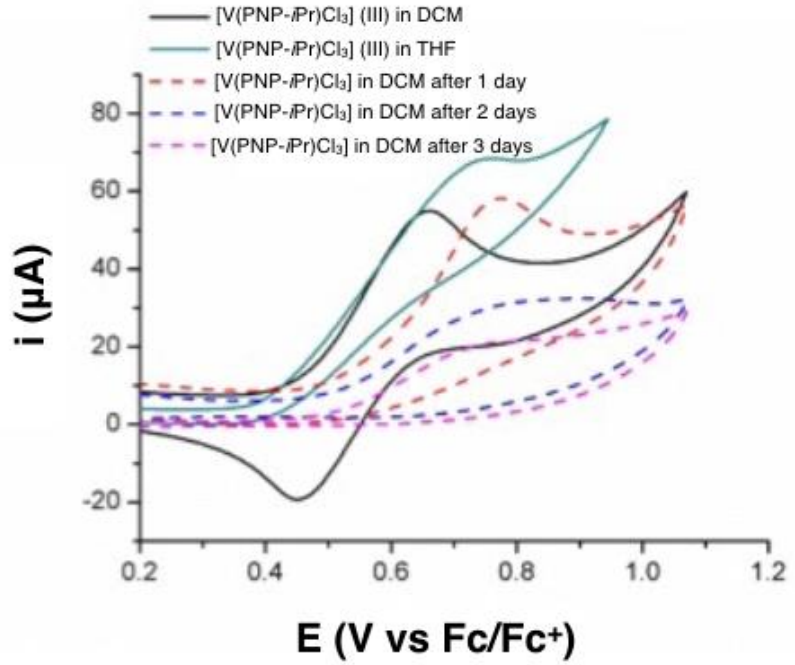

Figure 13 – Comparison of the cyclic voltammograms belonging to complex 3 in THF with CH_2Cl_2 after several days in the presence of air.

By providing an oxygen source to the CH_2Cl_2 solution of **3**, the voltammogram obtained after three days in contact with air (see Figure 13) converged to the voltammogram of the THF solution in the presence of nitrogen.

As shown in Scheme 1, [Ti(PNP-Ph_2)Cl_3] **5** was obtained in 54 % yield through reaction of **2** with $(THF)_3TiCl_3$. The paramagnetic complex **5** was characterized by IR spectroscopy as depicted in Figure 14.

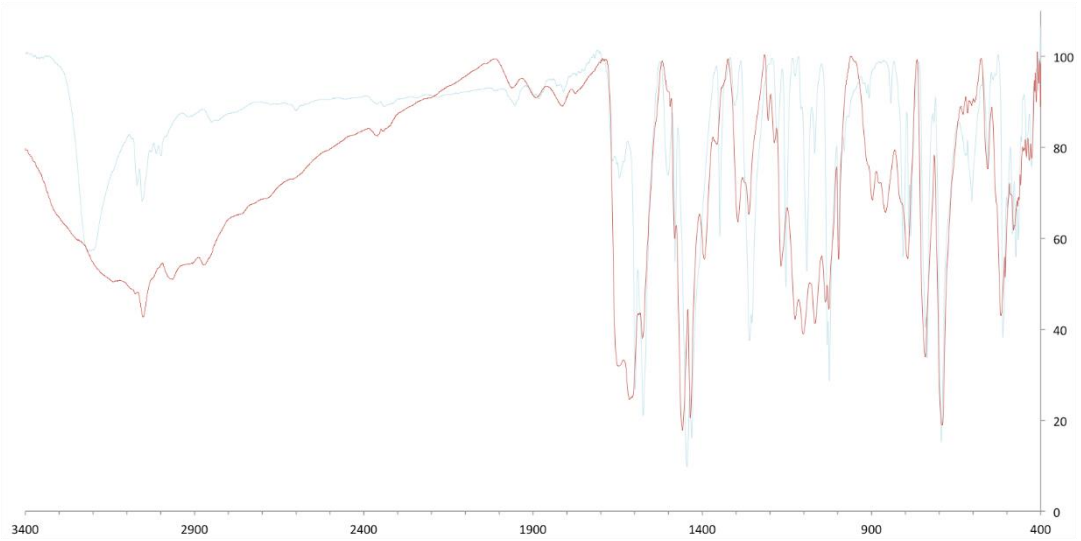

Figure 14 – Infrared spectra overlap between [Ti(PNP-Ph_2)Cl_3] (in red) and the respective ligand (in blue).

In the spectral region from 3400 to 2900 cm^{-1}, it is possible to find bands belonging to the P-N bond, the amine spacer and the phenyl group.

The characteristic pattern bands of mono substituted benzenes belonging to **5** can be found in the three bands at 1961, 1890 and 1814 cm^{-1}. The region of 1700 to 400 cm^{-1} displays several overlapped bands belonging to different frequencies of the pyridine backbone, the amine spacer and the phenyl group.

The comparison between the spectra of **2** and **5** shows two distinctive differences. Broader bands were formed and the spectral region of 1700 to 1000 cm^{-1} was moved to higher frequencies.

The reaction of **2** with $(THF)_{3.5}YCl_3$ gives the unexpected complex [Y(PNP-Ph_2)Cl_2][YCl_4] **6** that was obtained as a white solid in a low 34% yield. The formation of the cationic complex occurs independently of whether 1 or 2 equiv. of the yttrium precursor are used.

The ^{1}H NMR spectrum of complex **6** shows several overlapped resonances in the aromatic region attributed to the protons of the phenyl rings attached to the phosphines, the pyridine backbone and also the amino spacers of the PNP ligand. The ^{31}P and ^{13}C $\{^{1}H\}$ NMR spectra is also not conclusive due to the presence of several peaks

that might be attributed to the presence of two possible isomers of **6**. For these reasons, NMR characterization of **6** was not possible.

Complex **6** was characterized by IR spectroscopy as depicted in Figure 15. In the spectral region of 3500 to 3100 cm^{-1} it is possible to find a very intense broad band belonging to adventitious water. In accordance to this, the elemental analysis of the product revealed a mixture of water and **6** in the ratio 4:1, indicating the hygroscopic nature of this complex. Moreover, the ESI-MS spectrum of **6**, showed the only evident signal in the negative mode at m/z 231.24 that corresponds to the $[YCl_4]^-$ fragment. This result is in accordance with the formulation performed by EA that hints for the formation of a cationic complex of the type $[Y(PNP\text{-}Ph_2)Cl_2][YCl_4]$.

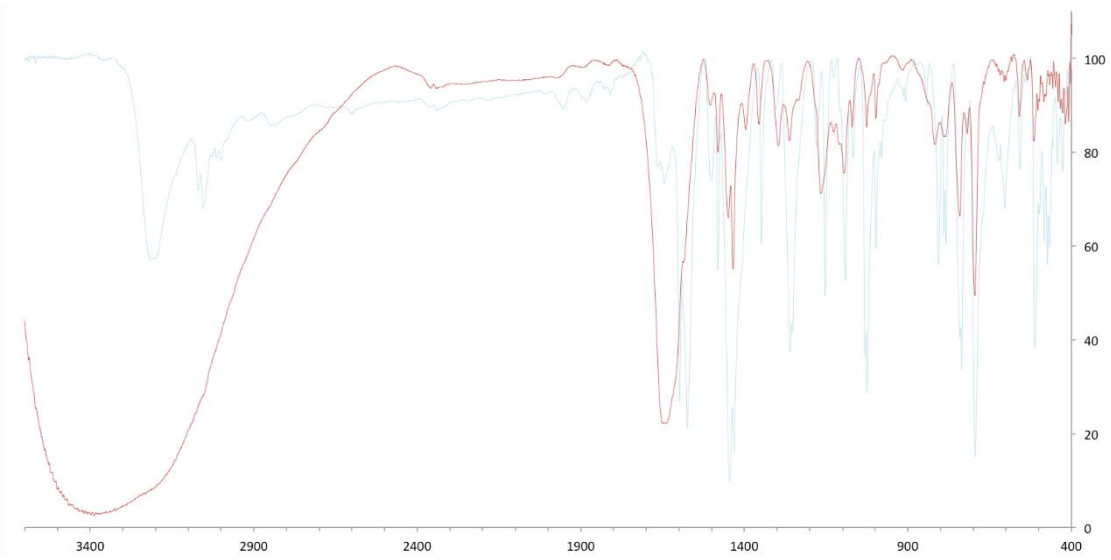

Figure 15 - Infrared spectra overlap between $[Y(PNP\text{-}Ph_2)Cl_2][YCl_4]$ (in red) and the respective ligand (in blue).

In Figure 15, the characteristic bands of mono substituted benzenes belonging to **4** can be found in the three bands at 1961, 1893 and 1822 cm^{-1}. The region of 1700 to 400 cm^{-1} displays several bands belonging to different frequencies of the pyridine backbone, the amine spacer and the phenyl group.

The wavelength region of 1650 to 400 cm^{-1} moved slightly to higher frequencies when compared with the organic precursor **2**. The bands became less intense, which may be due to a lower concentration of the analyzed sample.

In complexes **3** and **4** the presence of acidic protons bonded to the nitrogen may increase the susceptibility of the P-N bond towards hydrolysis under acidic or strongly basic conditions. A more robust ligand having a methyl group attached to the bridging nitrogen (N-CH_3) was also used for the synthesis of a V^{III} complex. PNP^{Me}-*i*Pr_2 was used to synthesize the complex [$V(PNP^{Me}$-$^{i}Pr_2)Cl_3$] **7** as shown in Scheme 3. [29]

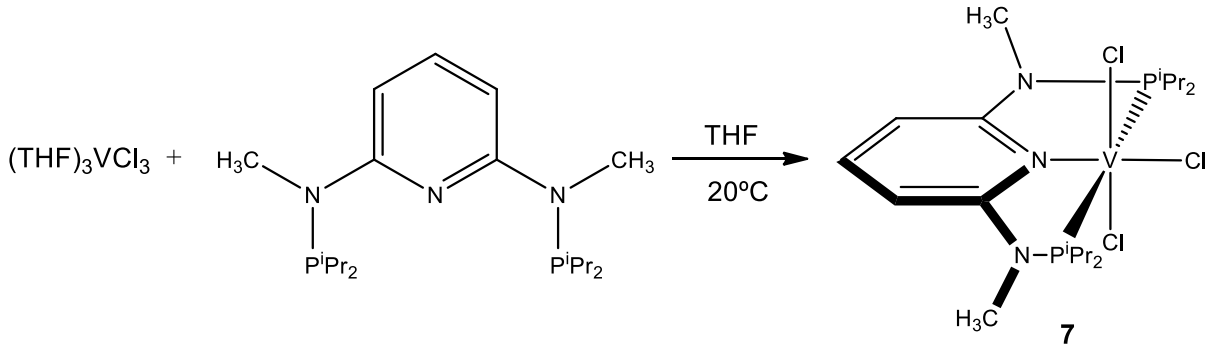

Scheme 3 – Synthesis of the vanadium complex [$V(PNP^{Me}$-$^{i}Pr)Cl_3$].

In accordance to the synthesis described for **3**, a green solid **7** was obtained in 68% yield, after removing the solvent under vacuum.

The paramagnetic complex [$V(PNP^{Me}$-$^{i}Pr)Cl_3$] **7** was characterized by IR spectroscopy, as depicted in Figure 16 . In terms of spectral regions, it is possible to find bands in the region from 2965 to 2873 cm^{-1} belonging to the methyl amine spacer, the P-N bond and to the aliphatic C-H stretching vibrations of the isopropyl group. The region of 1700 to 600 cm^{-1} displays several bands belonging to different frequencies of the pyridine ring, the isopropyl group and the methyl amine spacer.

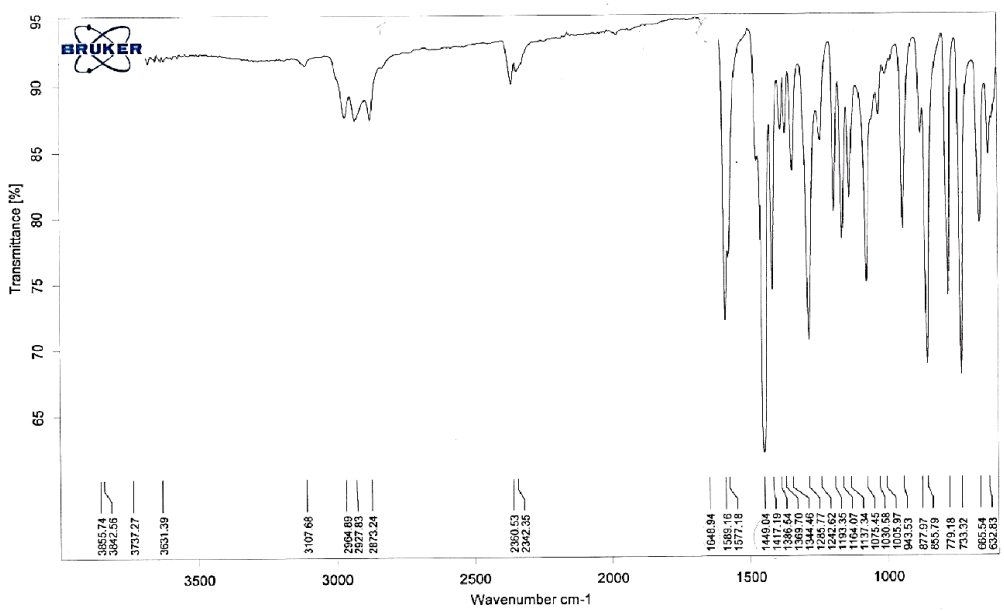

Figure 16 – Infrared spectrum of [V(PNP$^{Me\text{-}i}$Pr$_2$)Cl$_3$].

The comparison between the spectra of **7** and the organic precursor PNP$^{Me\text{-}i}$Pr$_2$ (spectrum not depicted) shows that the bands of the two spectral regions analysed before were moved to higher wavelength frequencies. In the region from 2965 to 2873 cm^{-1} the once broad band with medium intensity was replaced by a weak band while in the region of 1700 to 600 cm^{-1} the majority of the bands also had their intensity reduced, possibly due to a low complex concentration in the IR analysed sample. The band shift observed between the organic precursor and the complex spectra constitutes a pattern identical to the one observed in the parent vanadium, titanium and yttrium complexes, where the metal coordination implies a decrease in the energy of the ligand bonds, which originates an increase in the peak wavenumber.

The paramagnetic susceptibility of the vanadium complex **7** was determined by Evan's method. In acetone, the value obtained for $\boldsymbol{\mu_{eff,obs}}$ is 2.86, which compares well with the calculated value of 2.83, expected for the d^2 metal centre of 2e$^-$.

In addition to the previous characterization techniques, the solid-state molecular structure of complexes **3**, **4**, **5** and **7** was determined by single-crystal X-ray diffraction. Compound **3** crystalized in both monoclinic P(2)1/n and orthorhombic P2(1)2(1)2(1) space groups. The asymmetric unit of the latter contains two independent molecules **(3b1** and **3b2)**. Complexes **4** and **5** crystalize in a triclinic P-1 space group while

compound **7** crystallizes in an orthorhombic Pca21 space group with two independent molecules in the assymetric unit **(7a** and **7b)**. Other crystallographic and experimental details of data collection and crystal structure determinations are presented in the Appendix.

ORTEP representations are shown in Figures 17-20, for **3**, **4**, **5** and **7**, respectively. The correspondent relevant distances and angles are presented in Table 2. Details for the intermolecular hydrogen bonds are depicted in Table 3.

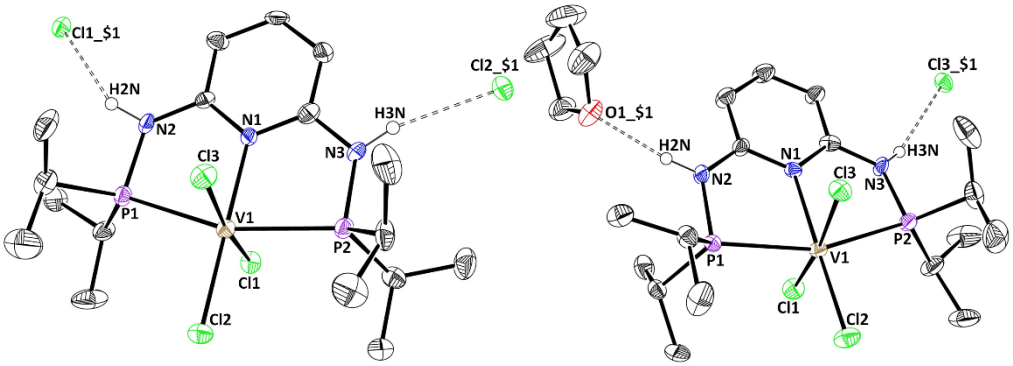

Figure 17 – ORTEP diagram of [V(PNP-^{i}Pr$_2$)Cl$_3$] showing thermal ellipsoids at 40% probability level. In 3a the hydrogen atoms and a co-crystallized CH_2Cl_2 molecule are omitted for clarity. In 3b the hydrogen atoms are omitted for clarity. The dashed lines represent hydrogen bonds.

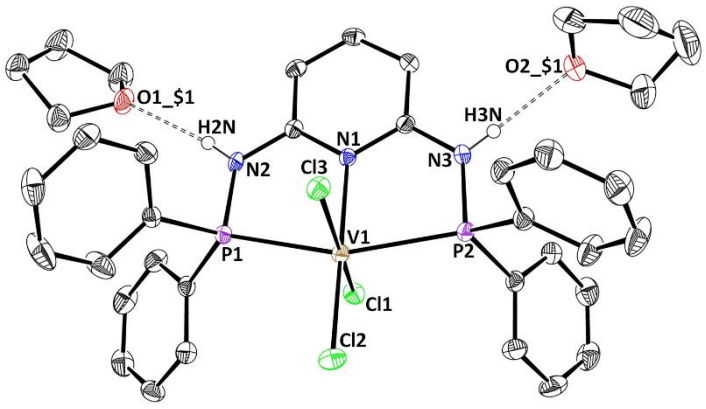

Figure 18 – ORTEP diagram of [V(PNP-Ph$_2$)Cl$_3$] showing thermal ellipsoids at 40% probability level. The hydrogen atoms are omitted for clarity.

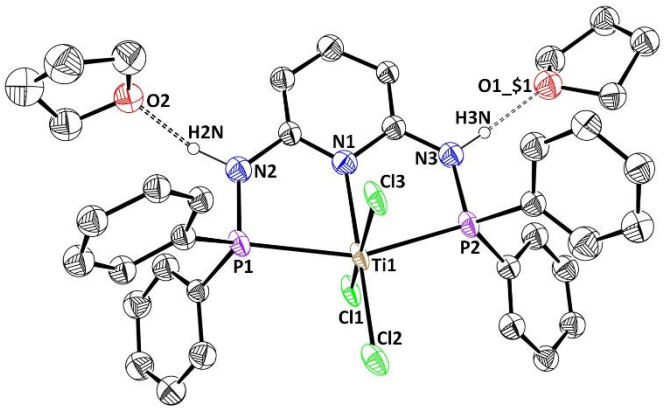

Figure 19 – ORTEP diagram of [Ti(PNP-Ph_2)Cl_3] showing thermal ellipsoids at 40% probability level. The hydrogen atoms are omitted for clarity.

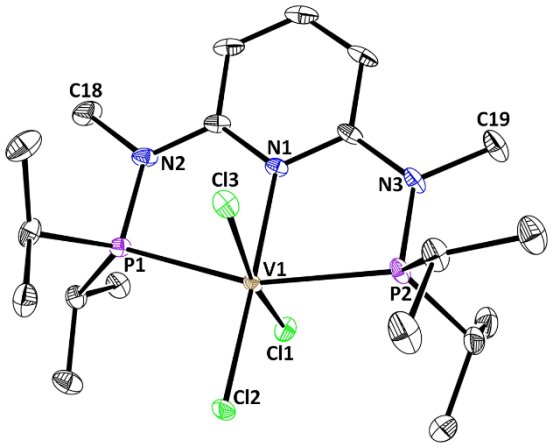

Figure 20 – ORTEP diagram of [V(PNP^{Me}-$^{i}Pr_2$)Cl_3] showing thermal ellipsoids at 40% probability level. The hydrogen atoms are omitted for clarity.

The geometries around the vanadium^{III} and titanium^{III} metal centres are best described as distorted octahedral. The three meridionally placed donor atoms of the PNP ligand and one chlorine atom occupy the equatorial plane of the octahedron. In all complexes the P-M-Cl angles are higher than 90° while the N-M-P bond angles are significantly more contracted (less than 90°) towards the pyridine ring. The other two chlorine atoms occupy the axial positions with the Cl-M-Cl (M=V,Ti) angles significantly deviated from linearity, attesting the octahedral distortion. In all structures, the M-P(1) bond and the M-P(2) bond distances are similar, except for **4** and **5** which shows a

difference of 0.028 and 0.0342 Å, respectively, between those bonds. This occurrence may be due to the steriochemical constraints inflicted by the phenyl substituents.

The two different solvomorphic structures of [V(PNP-^{i}Pr$_2$)Cl$_3$] were obtained from different solvent mixtures. Using a CH_2Cl_2/toluene system led to the formation of **3a** that displays a co-crystallized molecule of CH_2Cl_2 (Figure 17a). On the other hand, the THF/toluene system provided **3b** that contains one co-crystallized THF (Figure 17b). In **3a** two bond interactions of the type N-H•••Cl between the amino spacers and the chlorine atoms of two parent molecules are observed with distances of 2.585 and 2.433 Å. No interactions with the co-crystallized CH_2Cl_2 molecules were observed being these molecules occupying the voids of the supramolecular network. In **3b** a co-crystallized THF molecule is hydrogen bonded to one amino group of the PNP ligand while the other amino group displays a hydrogen bond with a chlorine atom from a neighbor molecule.

Table II – Selected bond lengths (Å) and angles (°) of the compounds [V(PNP-^{i}Pr$_2$)Cl$_3$], [V(PNP-Ph$_2$)Cl$_3$], [Ti(PNP-Ph$_2$)Cl$_3$], and [V(PNP^{Me}-^{i}Pr$_2$)Cl$_3$].

	3a	3b1	3b2	4	5	7a1	7a2
M-N(1)	2.140(5)	2.152(5)	2.159(4)	2.173(2)	2.22(1)	2.152(2)	2.156(1)
M-P(1)	2.494(2)	2.500(2)	2.470(2)	2.4738(7)	2.576(6)	2.4758(7)	2.4776(6)
M-P(2)	2.480(2)	2.501(2)	2.476(2)	2.5080(7)	2.548(5)	2.4767(7)	2.4703(7)
M-Cl(1)	2.366(2)	2.302(2)	2.390(2)	2.3098(7)	2.323(5)	2.3284(6)	2.3280(6)
M-Cl(2)	2.320(2)	2.286(2)	2.285(2)	2.2810(7)	2.365(6)	2.2856(6)	2.3041(7)
M-Cl(3)	2.301(2)	2.378(2)	2.286(2)	2.3261(7)	2.338(5)	2.3527(6)	2.3197(6)
P(1)-M-N(1)	79.6(2)	78.82(15)	79.83(15)	79.09(5)	76.7(4)	79.62(5)	79.65(5)
P(2)-M-N(1)	80.6(2)	79.49(15)	79.55(15)	78.48(5)	78.1(4)	79.47(5)	80.00(5)
P(1)-M-Cl(2)	100.65(8)	101.52(7)	99.34(7)	100.84(2)	102.48(19)	100.90(2)	100.05(2)
P(2)-M-Cl(2)	99.22(8)	100.19(7)	101.16(7)	101.62(3)	101.82(19)	100.00(2)	100.22(2)
Cl(1)-M-Cl(3)	171.38(8)	171.07(7)	168.11(7)	168.59(3)	168.7(2)	172.17(3)	168.15(2)

Once more, the disposition to form solvates is exhibited in the isostrutural complexes **4** and **5**. In both cases, two THF molecules interact with the NH spacers of

the PNP ligand by hydrogen bonds of the type N-H•••O. It is plausible that the stereochemical constraint created by the presence of the phenyl groups affects the formation of this type of structure, blocking the interaction with parent molecules, as observed in **3a** and **3b**. The absence of N-H groups in [V(PNP^{Me}-^{i}Pr$_2$)Cl$_3$] may justify the lack of co-crystallized solvent molecules in this compound.

Table III – Bond lengths (Å) for the intermolecular bonds.

	3a	**3b1**	**3b2**	**4**	**5**
N-H•••O	-	2.037	2.026	2.083	1.948
				2.062	1.946
N-H•••Cl	2.585	2.632	2.812	-	-
	2.433				

Reactivity Study

Oxidation reactions

Vanadium is highly oxophilic, with a tendency to form oxides by hydrolysis and abstraction of oxygen, allowing this metal to participate in a number of oxo-transfer reactions. [30, 31, 32]

Oxidation reactions of [V(PNP-^{i}Pr$_2$)Cl$_3$] **3** and [V(PNP-Ph$_2$)Cl$_3$] **4** with dried air were used to assess the possibility of forming metal oxo complexes.

A solution of [V(PNP-^{i}Pr$_2$)Cl$_3$] **3** in THF was stirred for six days under dried air. During the progress of the reaction, the initially green solution turned yellow after one day-and at the fourth day the reaction mixture change to dark red with a small amount of a white precipitate on the walls of the Schlenk. Since no further evolution was observed the precipitate was filtered off and the dark red solution was evaporated originating a green liquid. N-hexane was then added but nothing precipitated out of the mixture. Addition of Et$_2$O originated the appearance of a light green powder, which was separated by filtration and dried under vacuum.

The IR analysis of the product showed a spectrum similar to that of the starting complex, and the expected V=O bonds was not detected. In addition, bands at 1224 cm^{-1} and 533 cm^{-1} hinted at the presence of phosphine oxides. On other hand, the elemental analysis revealed a result with a similar value for the carbon composition but a nitrogen percentage of 3.43, significantly lower when compared with the starting complex value (7.81%).

The formation of crystalline material suitable for single crystal X-ray diffraction was attempted without success and the characterization of the product was not possible to achieve until now.

Figure 21 – Reaction progress in THF during the first, second, third, fifth and sixth days, respectively.

A reaction of **3** with dried air, similar to the one discussed above, was performed in CH_2Cl_2 and as before, several changes were observed along the time.

The initially brown solution turned dark green and an oily brown precipitate appeared at the bottom of the schlenk in the second day. In the following two days the solution became forest green maintaining the precipitate and finally, after 6 days of reaction a yellow solution with a large amount of a light green precipitate was formed. The precipitate was filtered off and solvent was removed under vacuum. The IR analysis of the product showed a very different spectrum comparing to the starting complex. The characteristic bands of the PNP-$^{i}Pr_2$ ligand were absent as well as any band assignable to a vanadium-oxo bond. Several changes in the region of 500 to 900 cm^{-1} could be noticed.

The formation of crystalline material suitable for single crystal X-ray diffraction was attempted without success and the characterization of the product was not possible until now.

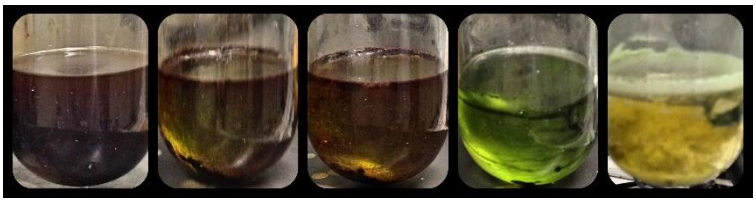

Figure 22 – Reaction progress in DCM during the first, second, third, fifth and sixth days, respectively.

Reduction reactions

Reduction reactions of [V(PNP-$^{i}Pr_2$)Cl_3] **3**, [V(PNP-Ph_2)Cl_3] **4** [V(PNP^{Me}-^{i}Pr)Cl_3] **7** were carried with several reducing agents to assess the halide abstraction with formation of vanadium^{II} and vanadium^{I} complexes.

[V(PNP-$^{i}Pr_2$)Cl_3] **3** does not react with $NaBH_4$, Zn or potassium naphtalenide in THF. Upon addition of any of those reagents no visible change takes place and the IR spectra of the products does not reveal any transformation compared with the starting complex.

NaK was added to a solution of [V(PNP-^{i}Pr$_2$)Cl$_3$] **3** in THF under CO atmosphere. The reaction mixture was left stirring overnight, originating a yellow solution with a white precipitate that was filtered off and discharged.

The IR analysis of the product obtained after solvent evaporation showed several modifications comparing to the starting complex although no CO bonding was detected. The region of 3054 to 2868 cm^{-1} belonging to the frequencies of the NH spacer and the isopropyl group was moved to lower wavelengths when compared to the starting complex **3**, alongside with the region of 1665 to 718 cm^{-1}. Unfortunately, these changes are not sufficiently elucidative and no crystals have been obtained to allow the identification of not product. The increase in the energy of the bonds represented by the decrease of the bands wavelength in the mentioned range may be suggestive of the abstraction of the acidic NH proton, with the formation of a C$_{Py}$=N double bond and de-coordination of the vanadium.

In a schlenk filled with CO and containing NaHg, [V(PNP^{Me}-^{i}Pr$_2$)Cl$_3$] **7** was added under a CO atmosphere. The reaction mixture was left stirring overnight, originating a brown solution (green at the beginning) with a grey precipitate, which was filtered off. The removal of the solvent under vacuum originated a red powder. In the IR analysis of the product no CO was detected. The spectrum obtained did not show any changes in the region of 600 to 1650 cm^{-1} and 2700 to 2900 cm^{-1} when compared with the starting complex, indicating that the reduction reaction proceeded differently from the reaction mentioned above. This result is not surprising since the N-methylated ligand has no acidic protons for abstraction but, as before, it was not possible to identify any compound.

Chloride abstraction reactions

Chlorine abstraction reactions of complexes **3** and **4** were carried using silver salts with the intent to form cationic complexes of V^{III}.

A brown mixture containing [V(PNP-^{i}Pr$_2$)Cl$_3$] and AgPF$_6$ in MeCN was stirred overnight at 50°C. The reaction mixture turned dark green with a white precipitate that was filtered off. After removing the solvent under vacuum, the brown powder obtained was analysed by IR spectroscopy. As revealed in Figure 22, the spectrum shows two

very considerable differences when compared with the starting complex **3**. A very broad band at 831 cm^{-1} suggests the presence of the anion PF^{6-} and a narrow band at 2291 cm^{-1} is indicative of the existence of acetonitrile.

Moreover, this reaction was also investigated by means of ESI-MS. In the positive mode, the second most abundant signal is observed at m/z equal to 448.34 which correspond to the complex $[Ag(PNP\text{-}^{i}Pr_2)]^{+}$, suggesting a transmetalation reaction.

Brown crystals were obtained from slow diffusion of a CH_2Cl_2 solution into toluene and characterized by single crystal X-ray diffraction, revealing the molecular structure of $[V(PNP\text{-}^{i}Pr_2)Cl_3]$.

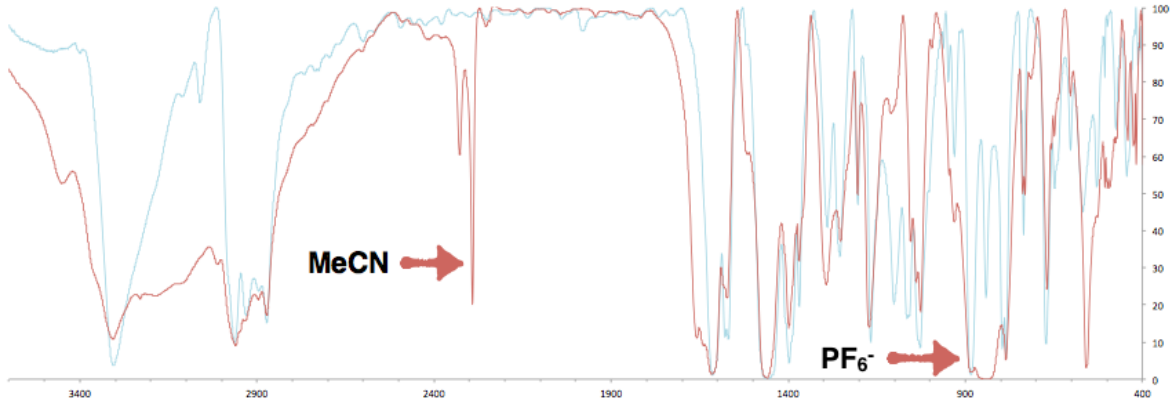

Figure 23 – Infrared spectra belonging to $[V(PNP\text{-}^{i}Pr_2)Cl_3]$ (blue) and to the product reaction (red).

Analogously to the previous reaction, $[V(PNP\text{-}^{i}Pr_2)Cl_3]$ was reacted with $AgPF_6$ and [(2,6-Me)Ph]NC in THF, forming a green solution. The use of isonitrile has the coordinating agent aims for the stabilization of the cationic species, not achieved in the previous reaction. After reacting overnight under reflux, the reaction mixture turned yellow with a purple precipitate that was filtered off. After removing the solvent under vacuum, an orange oil was obtained. The brown powder acquired through precipitation with diethyl ether was subject of IR spectroscopy. Once more, the spectrum shows two very considerable differences when compared with the starting complex **3**, a broad peak at 841 cm^{-1} suggests the presence of the anion PF^{6-} and a narrow medium peak at 2166 cm^{-1} is indicative of the presence of isonitrile.

The ESI-MS analysis of the product, in the negative mode, evidences the most abundant signal at m/z equal to 662.06 which correspond to the complex {Ag(PNP –

$iPr_2)[(2,6-Me)PhN](MeCN)_2\}^-$, resulting, once again, from ligand exchange between vanadium and silver. The acetonitrile comes from the solvent used to prepare the sample for mass analysis. In the positive mode, the most abundant signal at m/z equal to 478.22 corresponds to the complex $[V(PNP\text{-}^iPr_2)Cl_2O]^+$, followed by another oxygen containing cation, $[V(PNP\text{-}^iPr_2)Cl_2O_2]^+$ detected at m/z equal to 494.24.

To a green solution containing $[V(PNP\text{-}^iPr_2)Cl_3]$ in THF, an excess of both $AgPF_6$ and [(2,6-Me)Ph]NC was added. After refluxing overnight, the reaction mixture was yellow with a white precipitate that was filtered off. The solvent evaporation until dryness gave rise to a brown powder that was subject of IR spectroscopy. The spectrum obtained exhibited the presence of a broad peak at 842 cm^{-1} that suggest the presence of the anion PF^{6-}, and a narrow medium peak at 2166 cm^{-1}, indicative of the presence of isonitrile, as observed in the latter reaction.

The formation of crystalline material suitable for single crystal X-ray diffraction was obtained through diffusion of a solution of CH_2Cl_2 to toluene. Compound **8** cristallized has yellow crystals in a monoclinic I2/a space group, with half a molecule in the assymetric unit. An ORTEP depiction along with bond distances and angles are depicted in figure 24.

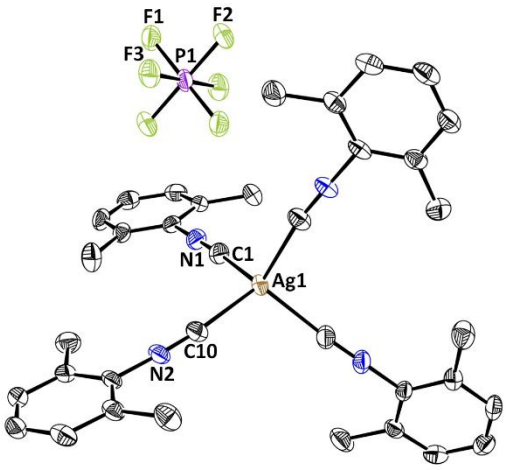

Figure 24 – ORTEP diagram of $[Ag((2,6\text{-}Me)PhNC)_4]$ $[PF_6]$ showing thermal ellipsoids at 40% probability level. The hydrogen atoms are omitted for clarity. Selected bond lengths (°) and bond angles(Å): Ag(1)-C(10) 2.211(3), Ag(1)-C(1) 2.215(3), N(1)-C(1) 1.151(4), N(2)-C(10) 1.154(3), C(10)-Ag(1)-C(10)#1 118.52(15), C(10)-Ag(1)-C(1)#1 109.29(10), C(10)#1-Ag(1)-C(1)#1 102.56(11), C(10)-Ag(1)-C(1) 102.56(11), C(10)#1-Ag(1)-C(1) 109.29(10), C(1)#1-Ag(1)-C(1) 115.20(15), C(1)-N(1)-C(2) 176.4(3), C(10)-N(2)-C(11) 176.8(3), N(1)-C(1)-Ag(1) 176.1(3), N(2)-C(10)-Ag(1) 171.5(3), P(1)-F(3) 1.5971(16), P(1)-F(1) 1.5985(16), P(1)-F(2) 1.6015(17), F(3)-P(1)-F(3)#2 180.00(12), F(3)-P(1)-F(1)#2 90.03(9).

The solid state molecular structure of **8** shows a silver^{I} complex in a distorted tetrahedral geometry. The four ligands occupy the vertices of the tetrahedron, with related Ag-C(1) and Ag-C(10) bond distances of 2.211(3) and 2.215(3) Å, respectively. These values match well with those found in silver^{I} complexes (for comparison, Ag-C bond length in Ag^{I} bipyridine complex 2.063) [33]. The C-Ag-C angles are deviated from 109.5° attesting the tetrahedral distortion observed. The N-C-Ag angles are also slightly distorted.

The PF_6^- anion displays a perfect octahedral geometry with a F(3)-P(1)-F(3)#2 angle of 180.00(12)° and the F(3)-P(1)-F(1)#2 angles of 90.03(9)°.

This molecular structure, together with the result of the ESI-MS of the latter reaction, is indicative of the preferential reaction of silver salts towards the formation of silver complexes.

Chloride Metathesis reactions

The reaction of [V(PNP-Ph_2)Cl_3] **4** and LiO^tBu in THF was left overnight forming a purple solution that was evaporated to dryness to give a purple solid. Addition of CH_2Cl_2 gave rise to a brown precipitate and a green solution. After removing the precipitate, the solution was evaporated to dryness and the green powder retrieved was subject of IR analysis, which showed a spectrum equal to the starting complex **4.** Crystalline material was obtained by diffusion of a THF solution into toluene. Single X-ray diffraction showed the molecular structure of [V(PNP-Ph_2)Cl_3]. This result suggests that in the presence of dichloromethane the alcoxide derivative initially formed is unstable, reverting to the starting complex.

A green solution containing [V(PNP-$^i Pr_2$)Cl_3] and 3 equivalents of LiO^tBu in THF was stirred overnight at room temperature. The reaction mixture turned dark green and an off-white precipitate appeared. The precipitate was filtered off and the solvent removed under vacuum. The resulting pink powder was analyzed by IR spectroscopy, which revealed a spectrum similar to the corresponding ligand. However, when

comparing the spectrum of this product with that of PNP-$^{i}Pr_2$, a new broad band with medium intensity at 952 cm^{-1} can be found, suggesting the presence of a V-O-V bond. [34]

The formation of crystalline material from the pink powder suitable for single crystal X-ray diffraction was obtained through diffusion of a THF solution into toluene. The compound crystallized in purple crystals in the monoclinic I2/a space group with half a molecule in the assymetric unit. An ORTEP depiction of $V(O^{t}Bu)_4(LiCl)_2(THF)_2$ **9** along with bond distances and angles are shown in Figure 24.

The molecular structure depicts a bimetallic compound with one vanadium^{IV} and two lithium metal centers in distorted tetrahedral geometries. The four bridging V-O-Li oxygen's occupy the vertices of the tetrahedron with O(1)-V and O(2)-V distances of 1.871(2) and 1.881(2) Å, respectively.

The O(1)-Li, O(2)-Li, O(3)-Li and Cl(1)-Li bond distances are 1.965(5), 1.978(6), 1.971(6) and 2.278(6) Å, respectively. These values match well with those found in other vanadium^{IV} complexes (for comparison, V-O bond lengths in other vanadium^{IV} octahedral complex 1.900(4), 1.917(4), 1.597(3) and 1.771(4) Å). [35] The V(1), O(1), Li(1) and O(2) atoms define two squares with internal angles close to 90°. The mean planes that contain the above mentioned atoms display a torsion angle of 87.77°. The presence of these two squares is responsible for the wider values found for the O(1)-V(1)-O(2)#1 and O(2)-V(1)-O(1)#1 angles that deviate from 109.5° as expected for a tetrahedral geometry. The same effect is observed for the lithium atom that displays also a distorted tetrahedral geometry. The supramolecular arrangement of $V(O^{t}Bu)_4(LiCl)_2(THF)_2$ shows a polymeric structure growing in the c direction by establishment of Li•••Cl interactions, with a bond length of 2.277 Å, as shown in Figure 25 B.

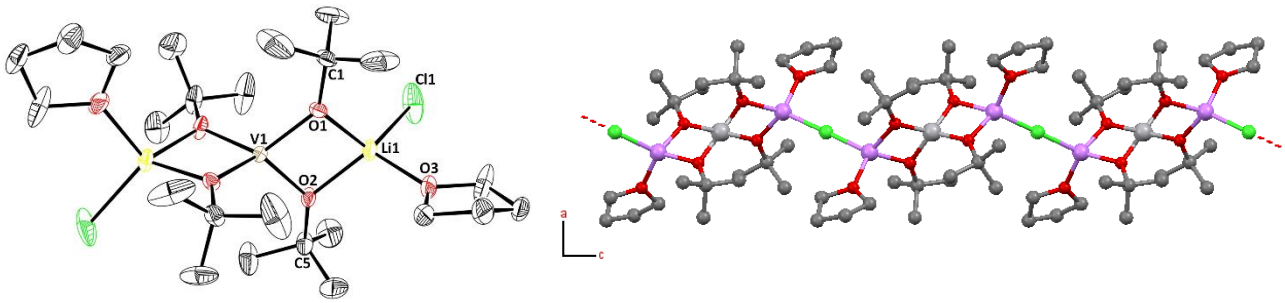

A B

Figure 25 – A: ORTEP diagram of $[V(O^tBu)_4(LiCl)_2(THF)_2]$ showing thermal ellipsoids at 40% probability level. The hydrogen atoms are omitted for clarity. Selected bond lengths (Å)and bond angles(°): Cl(1)-Li(1) 2.278(6), O(1)-V(1) 1.871(2), O(2)-V(1) 1.882(2), O(1)-Li(1) 1.965(5), O(2)-Li(1) 1.978(6), O(3)-Li(1) 1.971(6), Li(1)-V(1) 2.832 (5), V(1)-O(1)#2 1.871(2), V(1)-O(2)#2 1.881(2), V(1)-Li(1)#2 2.832(5), V(1)-O(1)-Li(1) 95.2(2), V(1)-O(2)-Li(1) 94.4(2), O(1)-Li(1)-O(3) 114.4(3), O(1)-Li(1)-O(2) 82.4(2), O(3)-Li(1)-O(2) 110.8(3), O(1)#2-V(1)-O(2)#2 87.62(8), O(1)-V(1)-O(2)#2 122.56(99), O(2)- V(1)-O(2)#2 120.8(1), Li(1)#2-V(1)-Li(1) 175.8(2). B : View along the b-axis of the supramolecular structure of $V(OtBu)_4(LiCl)_2(THF)_2$.

A green reaction mixture of $[V(PNP\text{-}^iPr_2)Cl_3]$ **3** and $LiNH^tBu$ in THF was stirred overnight, forming a dark red solution with a brown precipitate that was filtered off. The solvent was removed under vacuum resulting in a brown powder that was subject of IR analysis. The obtained spectrum revealed that the regions from 1616 to 670 cm^{-1} and from 2962 to 2870 cm^{-1} were kept in the same wavelength when compared with the starting complex spectrum. However, no characteristic signals can be identified in the region of 670 to 480 cm^{-1}.

The formation of crystalline material suitable for single crystal X-ray diffraction was attempted without success and the characterization of the product was not possible until now.

To conclude this work the reaction of **1** with a different vanadium precursor was subject of study. The addition of $VOCl_2•2H_2O$ to a solution of $PNP\text{-}^iPr_2$ **1** in THF, originated a blue solution that was stirred overnight. The solvent was removed under vacuum, originating a dark brown oil. The brown powder acquired trough precipitation with *n*-Hexane was subject of IR spectroscopy. In the region of 3200-2900 cm^{-1} a very intense broad band can be found belonging to water. Next to it, two bands at 2979 and

28172 cm^{-1} suggests the presence of the isopropyl group and the P-NH bond. The region below 1650 cm^{-1} shows several bands possibly belonging to different overlapped frequencies of the pyridine ring, the isopropyl group and the NH spacer. At 911 cm^{-1} a very strong band is found belonging to the V=O bond, distinctive of the vanadium precursor.

The reaction product spectrum shown considerable differences when compared with the organic precursor since the $VOCl_2 \bullet 2H_2O$ spectrum displays only two noticeable bands in the region below 1650 cm^{-1}. At 1634 cm^{-1} a broad band with strong intensity signals the presence of water while at 998 cm^{-1} band with medium intensity signals the presence of V=O.

The characterization of the reaction product was not achieved until now, since the formation of crystalline material suitable for single crystal X-ray diffraction was attempted without success. Nevertheless, a new reaction using the latter reaction product in THF was carried with the addition of a solution of triphenylphosphine in the same solvent. The reaction was stirred overnight forming a green solution with a white precipitate that was filtered off. The solvent was removed under vacuum resulting in a green powder that was subject of IR analysis. The obtained spectrum revealed in the region of 3700 cm^{-1} to 2500 cm^{-1} a very intense broad band that hints for the presence pf water. The region of 1653 to 400 cm^{-1} displays several changes when compared with the latter reaction spectrum, with highlight on the 800 to 400 cm^{-1} region that shows numerous new bands. At 996 cm^{-1} a very intense band appears, suggesting the presence of the V=O bond.

The formation of crystalline material suitable for single crystal X-ray diffraction was obtained through diffusion of a CH_2Cl_2 solution into Et_2O. The compound crystallized in the monoclinic P2(1)/n space group. An ORTEP depiction of $V(O)(Cl)_2(OPPh_3)_2$ **10** along with bond distances and angles are shown in Figure 25.

The molecular structure depicts a vanadium^{IV} complex with a square pyramidal geometry as attested by the τ value of 0.24 (the geometry around the metal centre is best described as a trigonal bipyramid if $\tau = 1$ or as a square pyramidal if $\tau = 0$).[36, 37] The two chlorine and the two oxygen atoms, O(1) and O(2), define the square of the pyramid. The oxygen atom (O(3)) occupies the apical position of the pyramid. The sum of the internal angles belonging to the square of the pyramid equals 345.3° revealing a slightly

distortion of the geometry, which can also be observed by the distance of 0.570 Å of the vanadium to the mean plane defined by Cl(1), Cl(2), O(1) and O(2). The V-Cl and V=O bond distances are within the values expected for this type of bonds, 2.294 and 1.607 Å, respectively. The P=O bond lengths of 1.504(2) and 1.497(2) Å are within the values found in other phosphine oxides (1.489 Å). Additionally the P-C bonds compares well with the value found for other triphenylphosphines 1.928 Å. [38]

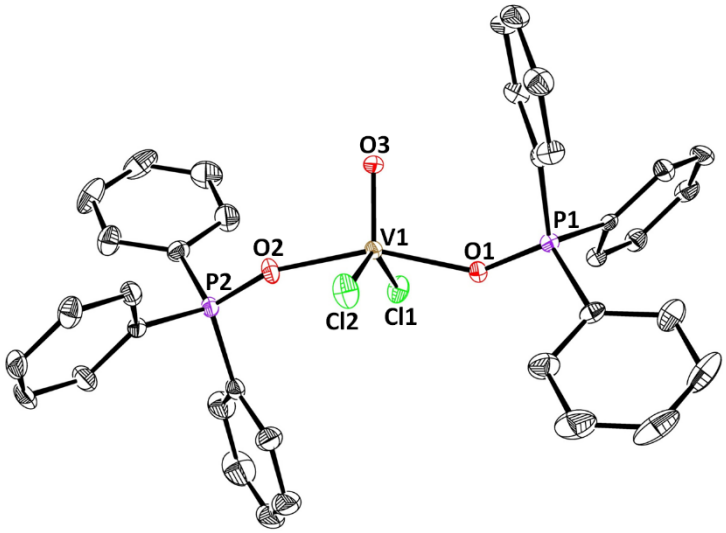

Figure 26 – ORTEP diagram of $[V(O)(Cl)_2(OPPh_3)_2]$ showing thermal ellipsoids at 40% probability level. The hydrogen atoms are omitted for clarity. Selected bond lengths (Å)and bond angles(°): V(1)-O(3) 1.5742(19), V(1)-O(2) 1.9890(19), V(1)-O(1) 1.9908(19), V(1)-Cl(1) 2.3215(8), V(1)-Cl(2) 2.3126(9), P(1)-O(1) 1.504(2), P(2)-O(2) 1.497(2), P(1)-C(1) 1.788(3), P(1)-C(13) 1.792(3), P(1)-C(7) 1.793(3), P(2)-C(31) 1.779(3), P(2)-C(19) 1.789(3), P(2)-C(25) 1.796(3); O(3)-V(1)-O(2) 100.93(10), O(3)-V(1)-O(1) 102.12(9), O(2)-V(1)-O(1) 156.91(8), O(3)-V(1)-Cl(2) 107.80(8), O(2)-V(1)-Cl(2) 88.29(6), O(1)-V(1)-Cl(2) 85.99(6), O(3)-V(1)-Cl(1) 109.64(8), O(2)-V(1)-Cl(1) 84.25(6), O(1)-V(1)-Cl(1) 86.77(6), Cl(5)-V(1)-Cl(1) 142.56(4), O(1)-P(1)-C(1) 113.48(12), O(2)-P(2)-C(31) 112.54(13), P(2)-O(2)-V(1) 156.50(13), P(1)-O(1)-V(1) 144.79(12).

Conclusion

In the present work early metal complexes based on PNP ligands of formulas [V(PNP-^{i}Pr$_2$)Cl$_3$], [V(PNP-Ph$_2$)Cl$_3$], [V(PNP^{Me}-^{i}Pr$_2$)Cl$_3$], [Ti(PNP-Ph$_2$)Cl$_3$] and [Y(PNP-Ph$_2$)Cl$_2$][YCl$_4$] have been prepared and characterized. The synthesis of all complexes was accomplished by treatment of MCl$_3$(THF)$_3$ (M=V and Ti) and YCl$_3$(THF)$_{3.5}$ with the respective PNP ligand. The complex [V(PNP-Ph$_2$)Cl$_3$] was also prepared without solvent through mechanochemistry. The solid state molecular structures of all V^{III} and Ti^{III} complexes were determined by single crystal X-ray diffraction showing octahedral geometries.

A preliminary study on the reactivity of the vanadium complexes was performed. Oxidation by dried air revealed the instability of the complexes and the affinity to form different products accordingly to the solvent used. Such species were observed by cyclic voltammetry but its full identification was not possible in the course of this work.

The reaction of the complex [V(PNP-^{i}Pr$_2$)Cl$_3$]with NaK under a CO atmosphere hints for the abstraction of the acidic NH proton, with the formation of a C$_{Py}$=N double bond and de-coordination of vanadium. However the reaction of the complex [V(PNP^{Me}-^{i}Pr)Cl$_3$] with NaHg under a CO atmosphere suggest that no reaction took place.

Chlorine abstraction reactions using silver salts revealed the formation of PNP silver species, which shows the propensity of the [V(PNP)Cl$_3$] complexes to undergo transmetallation reactions. Chloride methathesis reactions were tried with Li^{t}OBu but the isolation of the corresponding alkoxido derivatives was not possible. Still, the formation of a vanadium^{IV} complex of the type V(O^{t}Bu)$_4$(LiCl)$_2$(THF)$_2$ was verified in the reaction 3 equivalents of LiO^{t}Bu.

The reaction of PNP-^{i}Pr$_2$ with VOCl$_2$•2H$_2$O hints for the formation of a vanadyl species. In the presence of triphenylphosphine the later reaction led to the formation of V(O)(Cl)$_2$(OPPh$_3$)$_2$.

In conclusion, vanadium trichlorido complexes supported by PNP ligands based on 2,6-diaminopyridine display an unpredictable reactivity. The strong acidity of the metal center and the presence of a non-innocent NH spacer on the ligand might be related to this behaviour. The reactivity of the yttrium complexes based on the PNP

system should be further investigated because these species offers the advantage of being diamagnetic compounds. This characteristic will allow studying their reactivity by NMR, which was not possible for the V^{III} and Ti^{III} complexes.

Experimental Section

General Considerations

Unless otherwise stated, all manipulations were performed under an atmosphere of dry oxygen-free nitrogen by means of standard Schlenk and glovebox techniques. Solvents were pre-dried using 4 Å molecular sieves and refluxed over sodium-benzophenone (Et_2O, toluene and THF), CaH_2 (*n*-hexane, dichloromethane), P_2O_5 (acetonitrile) or sodium (methanol) under an atmosphere of N_2, and collected by distillation.

The compounds $(THF)_3VCl_3$, $(THF)_3TiCl_3$ and $(THF)_{3.5}YCl_3$ were prepared according to previously described procedures. [39, 40, 41] 2,6-diaminopyridine was purified by stirring the crude product over active charcoal in a solution of dichloromethane followed by filtration and solvent evaporation.

All other reagents were commercial grade and used without further purification.

Characterization Techniques

Cyclic Voltammetry

Sara Realista realized the cyclic voltammetry studies at Faculdade de Ciências da Universidade de Lisboa, Lisbon. All studies were realized at 25°C, at a constant rate of 100 mV s^{-1}. Dried nitrogen was bubbled in all solutions before any measurements. 0.1 M of $TBAPF_6$ was used as supporting electrolyte in complex solutions of 0.1 M. A three-electrode setup cell was used, established by a working electrode of platinum (3,14 mm^2), a reference electrode of SCE and a counter electrode of platinum foil (2 cm^2). The pair ferrocene/ferrocenium was used as internal pattern to measure the wave potential, in accordance with IUPAC recommendations.

Infrared Spectroscopy

Infrared spectra were recorded on a Jasco FT/IR – 410 spectrometer using KBr as support at CQE-IST and on a Perkin-Elmer 400 FIR FTIR spectrometer, equipped with a PikeTechnologies GladiATR using a diamond crystal plate at TU-Wien.

Elemental Analysis

Elemental analyses were obtained using a Fisions Instruments Mod EA-1108, from Laboratório de Análises do IST, Lisbon, Portugal. All samples were sent in glass ampules sealed under nitrogen atmosphere.

Nuclear Magnetic Ressonance

NMR spectra were recorded in a BRUKER AVANCE 300 MHz or 400 MHz spectrometer at 296 K, referenced internally to residual proton-solvent (^{1}H) resonances and reported relative to tetramethylsilane (0 ppm). ^{31}P was referenced to external H_3PO_4 (80%) (0 ppm).

Mass Spectrometry

Mass spectra (ESI-MS) were recorded by Dra. Conceição Oliveira, from CQE at IST, Lisbon, Portugal, on a Varian 500-MS ion trap mass spectrometer with nitrogen as nebulizer gas at 35.0 psi, and as drying gas at 350°C and 15.0 psi, capillary voltage of 80.0 and needle voltage of +5000 V.

Magnetic Susceptibility

Magnetic susceptibility measurements as function of Evan's Method were performed with a capillary with acetone as solvent in a BRUKER AVANCE 250 MHz and

300 MHz spectrometer at 296 K, referenced internally to residual proton-solvent (^{1}H) resonances and reported relative to tetramethylsilane (0 ppm).

Mechanochemistry

Mechanosynthesis was done at CQE-IST in a Retsch MM200 mill using a 10 mL acrylate milling jar and two milling balls made of stainless steel (10 mm diameter).

X-Ray Diffraction

Crystals suitable for single-crystal X-ray analysis were grown as described in the synthetic procedures.

Crystallographic data were collected at *Instituto Superior Técnico* by Doctor Luís Alves, under Doctor M. Teresa Duarte assistance. Crystals of air/moisture sensitive compounds were selected inside the glovebox, covered with polyfluroether oil and mounted on a nylon loop. The data were collected using a graphite monochromated Mo-K_α radiation (λ = 0.71073 Å) on a BRUKER AXS-KAPPA APEX II diffractometer equipped with an Oxford Cryosystem open-flow nitrogen cryostat. Cell parameters were retrieved using Bruker SMART software and refined using Bruker SAINT on all reflections. Absorption corrections were applied using SADABS. [42] The structures were solved and refined using the direct methods SIR92, SIR97 and SIR2004. [43, 44, 45] Structure refinement was done using SHELXL-97. [46] These programs are part of the WinGX software package version 1.80.01. [47] Torsion angles, mean square planes and other geometrical parameters were calculated using SHELX. [46] Unless stated otherwise, all non-hydrogen atoms were refined anisotropically and the hydrogen atoms were inserted in idealized positions and allowed to refine riding on the parent carbon atom. Illustrations of the molecular structures were made with ORTEP-3 for Windows. [48]

See the Appendix in this section for crystallographic experimental data and structure refinement parameters.

Ligand's Synthesis

1) N,N'-Bis(diisopropylphosphino)-2,6-diaminopyridine (PNP-$^{i}Pr_2$)[4]

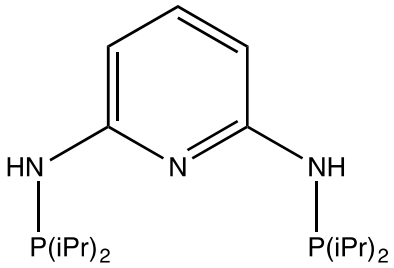

Triethylamine (2.64 mL, 18.7 mmol) was added to a suspension of 2,6-diaminopyridine (1.03 g, 9.43 mmol) in toluene (100 mL). The mixture was cooled at 0°C and P(*i*Pr)$_2$Cl (3.00 mL, 18.7 mmol) was added dropwise. The solution was allowed to reach room temperature and was refluxed overnight. The reaction mixture was then filtered and the solvent was removed under vacuum to give an yellow oil. The obtained oil was purified to give a withe crystalline solid **1** by flash chromatography, using silica gel (conditioned with 5 Vol% NEt_3) and 3:1 PE/EE, with EE as the eluent.

Yield: 2.62 g (81%) white crystalline solid; $C_{17}H_{33}N_3P_2$ (MW: 341.42);
^{1}H NMR (δ, $CDCl_3$, 20 °C): 7.23 (t, J = 8.1 Hz, 1H, py[4]), 6.42 (dd, J = 8.0 Hz, J = 2.1, 2H, py[3,5]), 4.48 (d, J = 10.7 Hz, H, NH), 1.72 (m, J = 7.0 Hz, J= 1.9 Hz, 4H, $CH(CH)_3)_2$, 1.07-0.97 (m, 24H, $CH(CH_3)_2$)
IR (cm^{-1}): 3340, (m.); 2950 (m.); 2865 (m.); 1582 (s.); 1444 (s.); 1384 (m.); 1347 (m.); 1278 (m.); 1245 (m.); 1148 (m.); 1099 (w.); 1079 (w.); 1012 (m.); 922 (w.); 878 (m.); 795 (m.); 780 (m.); 729 (m.); 664 (m.); 619 (m.); 567 (m.); 480 (m.); 441 (w.); 419 (w.).

2) N,N′-Bis(diphenylphosphino)-2,6-diaminopyridine (PNP-Ph_2)[4]

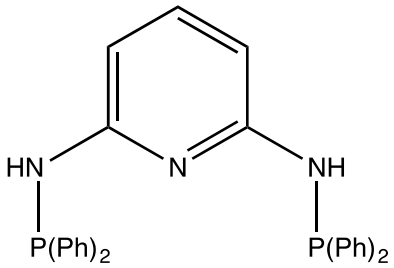

This ligand was prepared analogously to **2** with NEt3 (5.10 mL, 36.6 mmol), 2,6-diaminopyridine (2.00 g, 18.3 mmol) and $P(Ph)_2Cl$ (7.20 mL, 36.6 mmol) as starting materials. The obtained white solid **2** was purified by flash chromatography, using silica gel (conditioned with 5 Vol% NEt_3) and 1:1:1 PE/EE/DCM, with EE as the eluent.

Yield: 7.11 g (81%) white solid; $C_{29}H_{25}N_3P_2$ (MW: 477.49);
^{1}H NMR (δ, $CDCl_3$, 20 °C): 7.46-7.36 (m, 21H, Ph, py[4]), 6.53 (dd, J = 7.9 Hz, J = 1.2, 2H, py[3,5]), 5.47 (d, J = 8.2 Hz, 2H, NH);
IR (cm^{-1}): 3215 (m.); 3070 (w.); 3055 (w.); 1953 (w.); 1881 (w.); 1805 (w.); 1645 (m.); 1598 (s.); 1575 (s.); 1501 (m.); 1481 (m.); 1445 (vs.); 1431 (s.); 1348 (m.); 1304 (w.); 1260 (s.); 1179 (w.); 1153 (m.); 1092 (m.); 1025 (s.); 998 (w.); 907 (w.); 843 (w.); 807 (m.); 783 (m.); 736 (s.); 694 (s.); 604 (m.); 557 (m.); 512 (s.); 474 (m.); 443 (m.); 427 (m.).

Complexes' Synthesis

3) [V(PNP-$^{i}Pr_2$)Cl_3]

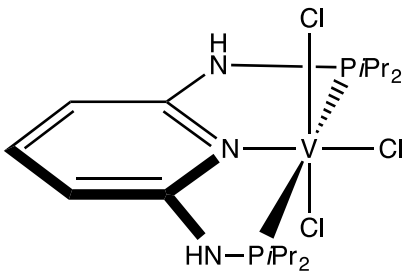

To a suspension of $(THF)_3V(Cl)_3$ (0.892 g, 2.41 mmol) in THF, PNP-$^{i}Pr_2$ (0.822 g, 2.41 mmol) was added. The reaction mixture was stirred for 2 hours at room temperature. The solvent was then removed under vacuum. The remaining brown solid was washed twice with toluene (10 mL) and twice with Et_2O (10 mL) and finally dried under vacuum. Brown crystals suitable for single crystal x-ray diffraction were obtained from diffusion of a THF solution into Toluene.

Yield: 867.30 mg (72%) brown solid; $C_{17}H_{33}Cl_3N_3P_2V$ (MW: 498.71);
IR (cm^{-1}): 3304 (vs.); 3060 (w.); 2963 (s.); 2930 (s.); 2872 (s.); 1613 (vs.); 1578 (s.); 1569 (s.); 1457 (vs.); 1398 (s.); 1369 (s.); 1290 (m.); 1254 (m.); 1203 (m.); 1167 (s.); 1102 (s.); 1065 (s.); 1028 (s.); 931 (m.); 884 (vs.); 841 (s.); 783 (s.); 736 (m.); 673 (s.); 603 (m.); 569 (m.); 529 (m.); 475 (m.); 444 (m.), 412 (w.).
ESI-MS (m/z): ESI (-) = 534.11 $[V(PNP\text{-}^{i}Pr_2)Cl_4]^-$, 498.13 $[V(PNP^{-H+}\text{-}^{i}Pr_2)Cl_3]^-$;
ESI (+) = 443.38 $[V(PNP\text{-}^{i}Pr_2)ClO]^+$, 462.20 $[V(PNP\text{-}^{i}Pr_2)Cl_2]^+$.
Elemental Analysis calculated for $C_{17}H_{33}Cl_3N_3P_2V\cdot 0.5(Et_2O)$ (%): N = 7.84, C = 42.59, H = 7.15. Found: N = 7.81, C = 42.56, H = 7.31.

4) [V(PNP-Ph_2)Cl_3]

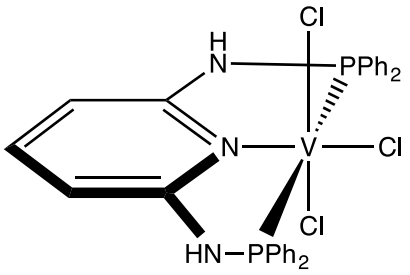

To a suspension of $(THF)_3V(Cl)_3$ (1.56 g, 4.19 mmol) in THF, PNP-Ph_2 (2.00 g, 4.19 mmol) was added. After the reaction mixture was stirred for 2 hours at room temperature, the precipitate formed was filtered off and the solvent was removed under vacuum. The remaining green solid was washed twice with toluene (10 mL) and twice with Et_2O (10 mL) and finally dried under vacuum. Green crystals suitable for single crystal x-ray diffraction were obtained from diffusion of a THF solution into Toluene.

Yield: 1.60g (60%) green solid; $C_{29}H_{25}Cl_3N_3P_2V$ (MW: 634.78);
IR (cm^{-1}): 3278 (s.); 3177 (s.); 3054 (s.); 2974 (s.); 2915 (s.); 2875 (s.); 1964 (w.); 1891 (w.); 1815 (w.); 1611 (vs.); 1577 (vs.); 1456 (vs.); 1436 (vs.); 1391 (s.); 1332 (m.); 1298 (m.); 1209 (m.); 1169 (s.); 1103 (vs.); 1040 (vs.); 998 (s.); 894 (s.); 854 (s.); 789 (s.); 735 (s.); 695 (s.); 632 (m.); 582 (m.); 521 (vs.); 484 (s.); 404 (w.).
ESI-MS (m/z): ESI (-) = 669.33 $[V(PNP\text{-}Ph_2)Cl_4]^-$; 632.18 $[V(PNP^{-H+}\text{-}Ph_2)Cl_3]^-$;
ESI (+) = 579.12 $[V(PNP\text{-}Ph_2)ClO]^+$.
Elemental Analysis calculated for $C_{29}H_{25}Cl_3N_3P_2V \cdot 0.56(Et_2O) \cdot 0.31(C_7H_8)$ (%):
N = 5.97, C = 56.9, H = 4.76. Found: N = 5.68, C = 56.88, H = 4.56.

4) Mechanosynthesis of [V(PNP-Ph_2)Cl_3]

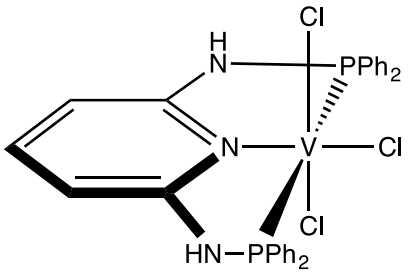

A mixture of [V(PNP-Ph_2)Cl_3] (100 mg, 0.209 mmol) and $(THF)_3VCl_3$ (70.5 mg, 0.190 mmol) was milled for 10 minutes under a nitrogen atmosphere, after which the colour changed from pink to green. The reaction vessel was opened under a nitrogen atmosphere, and the product was transferred to a Schlenk. A green powder was obtained after being washed twice with toluene and dried under vacuum.

Elemental Analysis calculated for $C_{29}H_{25}Cl_3N_3P_2V\cdot(THF)_3VCl_3$ (%): N = 4.18,
C = 48.98, H = 4.61.
Found: N = 4.56, C = 46.71, H = 3.48.

5) [Ti(PNP-Ph_2)Cl_3]

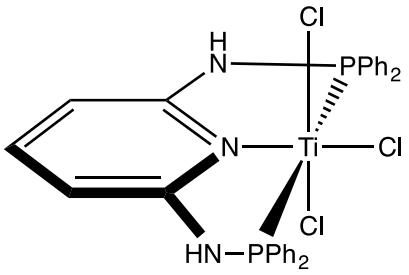

This complex was prepared analogously to **2** with $(THF)_3Ti(Cl)_3$ (175 mg, 0.496 mmol), PNP-Ph_2 (250 mg, 0.524 mmol) as starting materials, with the exception that the reaction mixture was refluxed overnight. Brown crystals suitable for single crystal x-ray diffraction were obtained from diffusion of a THF solution into Toluene.

Yield: 162 mg (54%) brown solid; $C_{29}H_{25}Cl_3N_3P_2Ti$ (MW: 631.70);
IR (cm^{-1}): 3051 (m.); 2966 (m.); 2871 (m.); 1961 (w.); 1890 (w.); 1814 (w.); 1645 (s.); 1616 (s.); 1577 (s.); 1458 (s.); 1435 (s.); 1394 (m.); 1295 (m.); 1262 (m.); 1167 (m.); 1102 (m.); 1067 (m.); 1036 (m.); 1026 (m.); 997 (m.); 897 (m.); 858 (m.); 793 (m.); 742 (s.); 691 (vs.); 557 (m.); 518 (s.); 480 (m.).
ESI-MS (m/z): ESI (-) = 662.07 $[Ti(PNP\text{-}Ph_2)Cl_4]^-$.
Elemental Analysis calculated for $C_{29}H_{25}Cl_3N_3P_2Ti \cdot H_2O$ (%): N = 6.47, C = 53.61, H = 4.19.
Found: N = 4.90, C = 54.04, H = 4.75.

6) $[Y(PNP\text{-}Ph_2)Cl_2]YCl_4$

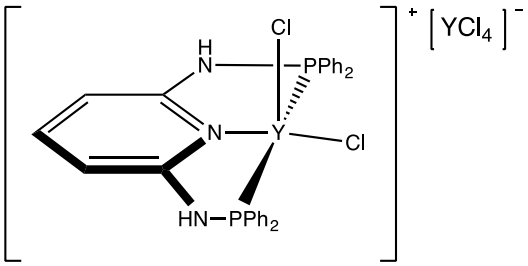

This complex was prepared analogously to **3** with $(THF)_{3.5}Y_3(Cl)_3$ (542 mg, 0.611 mmol), PNP-Ph_2 (291 mg, 1.22 mmol) as starting materials, with the exception that the reaction mixture was refluxed overnight.

Yield: 91 mg (23%) white solid; $C_{29}H_{25}Cl_6N_3P_2Y_2$ (MW: 868);
IR (cm^{-1}): 3388 (vs.); 1961 (w.); 1893 (w.); 1822.4 (w.); 1639 (s.); 1480 (w.); 1449 (m.); 1434 (m.); 1395 (w.); 1355 (w.); 1295 (w.); 1262 (w.); 1166 (m.); 1094 (m.); 1070 (w.); 1026 (w.); 997 (w.); 818 (w.); 741 (m.); 695 (m.); 558 (w.); 514 (w.); 484 (w.);
ESI-MS (m/z): ESI (-) = 231.24 $[YCl_4]^-$.
Elemental Analysis calculated for $C_{29}H_{25}Cl_6N_3P_2Y_2 \cdot 2H_2O$ (%): N = 4.47, C = 37.05, H = 3.54.
Found: N = 4.40, C = 36.65, H = 3.84.

7) [V(PNP$^{Me\text{-}i}$Pr$_2$)Cl$_3$]

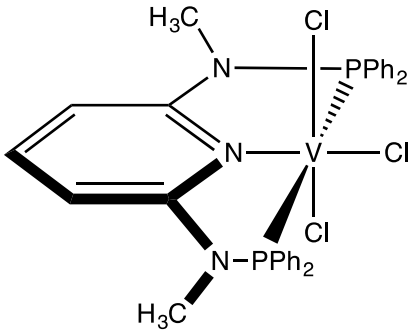

This complex was prepared analogously to **3** with (THF)$_3$V(Cl)$_3$ (402 mg, 1.09 mmol) and PNP$^{Me\text{-}i}$Pr$_2$ (400 mg, 1.09 mmol) as starting materials. Crystals suitable for single crystal x-ray diffraction were obtained from diffusion of Et$_2$O into a THF solution.

Yield: 389 mg (68%) green solid; $C_{19}H_{37}Cl_3N_3P_2V$ (MW: 526.77);
IR (cm^{-1}): 2965 (w.); 2928 (w.); 2873 (w.); 1649 (s.); 1449 (vs.); 1417 (s.); 1387 (w.); 1370 (w.); 1344 (w.); 1286 (s.); 1286 (w.); 1243 (m.); 1193 (m.); 1164 (m.); 1137 (m.); 944 (m.); 856 (s.); 779 (s.); 733 (s.); 666 (m.); 633 (w.).

Oxidation Reactions

Reaction of [V(PNP-^{i}Pr$_2$)Cl$_3$] in THF with dried air

A solution of **3** (250 mg, 0.5 mmol) in 20 mL of THF was stirred for six days under dried air using a $CaCl_2$ guard tube. The initially green solution turned yellow after one day–and at the fourth day the reaction mixture change to dark red with a small amount of a white precipitate on the walls of the Schlenk. The precipitate was filtered off and the dark red solution was evaporated originating a green liquid. N-hexane was added for precipitation without success. Addition of Et_2O originated the appearance of a light green powder, which was separated by filtration and dried under vacuum.

IR (cm^{-1}): 3420 (w.); 2962 (m.); 2935 (m.); 2874 (m.); 2359 (w.); 1718 (m.); 1684 (m.); 1600 (m.); 1466 (m.); 1386 (w.); 1367 (w.); 1273 (w.); 1171 (s.); 1133 (vs.); 1065 (vs.); 1032 (s.); 1002 (s.); 928 (w.); 887 (m.); 795 (w); 715 (m.); 578 (w.); 502 (w.); 432 (m.).

Reaction of [V(PNP-Ph$_2$)Cl$_3$] in CH_2Cl_2 with dried air

A solution of **3** (250 mg, 0.5 mmol) in 20 mL of CH_2Cl_2 was stirred for six days under dried air using a $CaCl_2$ guard tube. The initially brown solution turned dark green and an oily brown precipitate appeared at the bottom of the Schlenk in the second day. In the following two days the solution became forest green maintaining the precipitate. After 6 days of reaction a yellow solution with a large amount of a light green precipitate was formed. The precipitate was filtered off and solvent was removed under vacuum.

IR (cm^{-1}): 3079 (s.); 2972 (s.); 2936 (s.); 2876 (s.); 2823 (s.); 2744 (s.); 1639 (vs.); 1610 (vs.); 1560 (s.); 1507 (w.); 1462 (s.); 1430 (s.); 1394 (w.); 1356 (s.); 1330 (w.); 1259 (m.); 1224 (s.); 1169 (vs.); 1144 (s.); 1100 (s.); 1025 (vs.); 1008 (s.); 984 (m.); 905 (s.); 882 (s.); 835 (m.); 806 (s.); 721 (m.); 683 (m.); 597 (w.); 532 (s.); 468 (w.).

Reduction Reactions

Reaction of [V(PNP-^{i}Pr$_2$)Cl$_3$] with Zn (3 equiv.)

To a green solution of **3** (250 mg, 0.503 mmol) in 10 mL of THF, Zn (98.8 mg, 1.51 mmol) was added. After being stirred overnight, no change in the reaction mixture appearance was verified. The solvent was removed under vacuum, and the remaining brown solid product was extracted from the zinc salts with acetone.

IR (cm^{-1}): 3297 (m.); 2964 (w.); 2931 (w.); 2873 (w.); 1612 (m.); 1578 (m.); 1456 (vs.); 1397 (m.); 1369 (w.); 1292 (w.); 1253 (w.); 1166 (m.); 1101 (m.); 1058 (m.); 1027 (m.); 883 (s.); 843 (w.); 787 (m.); 735 (m.); 671 (m.).

Reaction of [V(PNP-^{i}Pr$_2$)Cl$_3$] with NaBH$_4$ (2.5 equiv.)

To a green solution of **3** (150 mg, 0.302 mmol) in 10 mL of THF, NaBH$_4$ (28.5 mg, 0.755 mmol) was added. The reaction mixture was stirred overnight, displaying no changes in the next day. The solvent was removed under vaccum disclosing a brown powder.

IR (cm^{-1}): 3493 (m.); 3493 (w.); 3432 (w.); 2965 (w.); 1560 (m.); 1458 (s.); 1033 (m.); 884 (m.); 788 (w.); 706 (m.); 629 (m.).

Reaction of [V(PNP-Ph$_2$)Cl$_3$] with Potassium Naphtalanide

To a suspension of naphtalanide (25.7 mg, 0.201 mmol) in 5 mL of THF, potassium (4.61 mg, 0.201 mmol) was added. The reaction mixture was stirred for 2 hours until all of the potassium metal was dissolved, forming a dark green solution, to which **3** (100 mg, 0.201 mmol) was added. After 3 days reacting, no change in the reaction mixture was observed. The solvent was removed under vacuum, forming a green powder.

IR (cm^{-1}): 3215 (m.); 1598 (m.); 1574 (m.); 1445 (s.); 1348; 1260 (w.); 1153 (w.); 1092 (w.); 1025 (m.); 998 (m.); 918 (w.); 806 (w.); 784 (m.); 735 (m.); 693 (vs.).

Reaction of [V(PNP-^{i}Pr$_2$)Cl$_3$] with NaK (4 equiv.) under a CO atmosphere

3 (66 mg, 0.13 mmol) was dissolved in 15 mL of THF and, and NaK (19 mg, 0.53 mmol) was added. CO was bubbled trough the solution for 5 minutes and the reaction mixture was then stirred under CO atmosphere overnight. The solvent was removed from the yellow solution under vaccum and the yellow powder was washed with Et_2O.

IR (cm^{-1}): 3054 (m.); 2957 (m.); 2925 (m.); 2868 (m.); 1665 (w.); 1552 (m.); 1424 (vs.); 1356 (m.); 1265 (m.); 1265 (m.); 1112 (m.); 1067 (s.); 1025 (m.); 915 (w.); 883 (w.); 818 (w.); 750 (w.); 720 (w.).

Reaction of [V(PNP^{Me}-^{i}Pr$_2$)Cl$_3$] with NaHg (excess) under a CO atmosphere

To a suspension of sodium (26.2 mg, 1.14 mmol) in 5 mL of THF, mercury (262 mg, 1.31 mmol) was added. The reaction mixture was stirred for 1 hour. Subsequently, CO was bubbled trough the suspension and **7** (100 mg, 0.19 mmol) was added, whereupon the colour of the solution turned to dark green alongside with a white precipitate. The reaction was then stirred overnight under CO atmosphere. The silver precipitate formed was filtered off and the solvent was removed under vaccum, disclosing a red powder.

IR (cm^{-1}): 2874 (m.); 1590 (s.); 1417 (m.); 1388 (w.); 1369 (w.); 1349 (w.); 1285 (m.); 1243 (m.); 1191 (m.); 1164 (m.); 1134 (m.); 1075 (m.); 941 (m.); 857 (s.); 788 (m.); 777 (m.); 732 (s.); 669 (m.); 633 (m.).

Chloride Abstraction Reactions

Reactions of [V(PNP-^{i}Pr$_2$)Cl$_3$] with AgPF$_6$:

In MeCN

A mixture of **3** (250 mg, 0.5 mmol) with AgPF$_6$ (127 mg, 0.5 mmol) was dissolved in 10 mL of MeCN forming a brown solution. The reaction mixture was stirred overnight at 50°C, whereupon the colour of the solution turned to dark green with a withe precipitate that was filtered off. The solvent was removed under vacuum disclosing a brown powder. Brown crystals suitable for single crystal x-ray diffraction were obtained from diffusion of a CH_2Cl_2 solution into Toluene.

IR (cm^{-1}): 3451 (m.); 3306 (s.); 2961 (s.); 2872 (s.); 2328 (m.); 2292 (m.); 2253 (w.); 1658 (s.); 1617 (vs.); 1573 (s.); 1459 (vs.); 1398 (s.); 1369 (m.); 1292 (m.); 1252 (m.); 1204 (m.); 1172 (s.); 1054 (m.); 1038 (m.); 1026 (s.); 931 (m.); 1038 (s.); 1026 (s.); 931 (m.); 831 (vs.); 785 (vs.); 731 (m.); 669 (s.); 559 (vs.); 492 (m.); 442 (m.); 418 (m.);
ESI-MS (m/z): ESI (+) **=** 443.41 [V(PNP-^{i}Pr$_2$)ClO]$^{+}$; 448.34[Ag(PNP-^{i}Pr$_2$)]$^{+}$;
462.20 [V(PNP-^{i}Pr$_2$)Cl$_2$]$^{+}$.
Elemental Analysis calculated for $C_{19}H_{36}Cl_2N_4P_2V$ (%): N = 11.11, C = 45.25, H = 7.20. Found: N = 7.46, C = 44.61, H = 6.72.

In THF with the presence of isonitrile

A mixture of **3** (211 mg, 0.425 mmol) with AgPF$_6$ (107 mg, 0.425 mmol) and isonitrile (55.7 mg, 0.425 mmol) was dissolved in 10 mL of THF forming a green solution. The reaction mixture was stirred overnight at 90C, whereupon the colour of the solution turned to yellow with a purple precipitate that was then filtered off. The solvent was removed under vacuum disclosing an orange oil. After precipitation with 40 mL of Et_2O, the brown powder was dried under vacuum.

IR (cm^{-1}): 3446 (m.); 3359 (m.); 3202 (m.); 2962 (s.); 2872 (m.); 2166 (m.); 1658 (s.); 1609 (s.); 1462 (s.); 1388 (w.); 1359 (w.); 1297 (m.); 1262 (m.); 1171 (m.); 1100 (m.); 1025 (m.); 933 (w.); 842 (vs.); 785 (s.); 739 (w.); 674 (w.); 558 (s.); 498 (m.); 441 (w.); 417 (w.); 404 (w.);

ESI-MS (m/z): ESI (-) **=** 662.06 $[Ag(PNP\text{-}^{i}Pr_2)(MeCN)_2((2,6\text{-}Me)PhNC]^-$;

ESI (+) **=** 478.22 $[V(PNP\text{-}^{i}Pr_2)Cl_2O]^+$; 494.24 $[V(PNP\text{-}^{i}Pr_2)Cl_2O_2]^+$.

Elemental Analysis calculated for $C_{26}H_{42}Cl_2N_4P_2V$ (%): N = 9.43, C = 52.53, H = 7.12. Found: N = 5.81, C = 35.09, H = 5.31.

In THF with the presence of an excess of isonitrile and $AgPF_6$

This reaction proceeded analogously to the last reaction. From **3** (211 mg, 0.42 mmol) with silver salts (507 mg, 2 mmol) and isonitrile (263. mg, 2 mmol) in THF. Crystals suitable for single crystal x-ray diffraction were obtained from diffusion of a CH_2Cl_2 solution into Toluene.

IR (cm^{-1}): 3449 (m.); 3333 (m.); 3081 (s.); 2917 (s.); 2872 (m.); 2229 (m.); 2166 (m.); 1658 (s.); 1613 (vs.); 1518 (s.); 1393 (s.); 1359 (m.); 1295 (m.); 1262 (m.); 1209 (m.); 1189 (s.); 1025 (m.); 1013 (m.); 952 (m.); 842 (vs.); 785 (m.); 734 (m.); 654 (w.); 558 (s.); 497 (m.); 441 (w.); 417 (w.); 406 (w.);

Metathesis Reactions

Reaction of [V(PNP-Ph_2)Cl_3] with LiO^{t}Bu

To a solution of **4** (250 mg, 0.394 mmol) in THF, a suspension of LiOtBu (31.5 mg, 0.394 mmol) in THF was slowly added. The reaction mixture was stirred overnight, whereupon the colour of the solution turned to purple with a green precipitate that was then filtered off. The solvent was removed under vacuum forming purple oil. After the oil precipitation with 40 mL of DCM, the green solution was dried under vacuum. Green crystals suitable for single crystal x-ray diffraction were obtained from the diffusion of a THF solution into Toluene.

IR (cm^{-1}): 3045 (w.); 2360 (w.); 1611 (m.); 1461 (vs.); 1436 (m.); 1394 (w.); 1262 (w.); 1103 (m.); 1040 (m.); 896 (w.); 794 (m.); 742 (m.); 691 (m.); 520 (m.); 481 (m.); 444 (m.); 435 (m.); 402 (w.).

Reaction of [V(PNP-^{i}Pr_2)Cl_3] with LiO^{t}Bu (3 equiv.)

To a solution of **3** (250 mg, 0.501 mmol) in THF, a suspension of LiOtBu (120 mg, 1.50 mmol) in THF was slowly added. The reaction mixture was stirred overnight. Afterwards, the solids were filtered off and the solvent was removed under vacuum. The pink solid obtained was dried under vacuum. Purple crystals suitable for single crystal x-ray diffraction were obtained from solvent diffusion THF/Toluene.

IR (cm^{-1}): 3243 (s.); 2967 (s.); 2926 (s.); 2866 (s.); 1603 (s.); 1583 (s.); 1499 (m.); 1447 (vs.); 1382 (m.); 1359 (s.); 1290 (m.); 1275 (s.); 1241 (m.); 1154 (s.); 1101 (w.); 1088 (w.); 1049 (m.); 1029 (s.); 953 (s.); 879 (m.); 803 (s.); 782 (s.); 732 (w.); 665 (m.); 613 (s.); 487 (m.); 448 (w.); 418 (w.).

Reaction of [V(PNP-^{i}Pr_2)Cl_3] with LiNH^{t}Bu

To a solution of **3** (250 mg, 0.503 mmol) in THF, a suspension of LiNH^{t}Bu (39.8 mg, 0.503 mmol) in THF was slowly added. The reaction mixture was stirred overnight, whereupon the colour of the solution turned to purple with a green precipitate that was

then filtered off. The solvent was removed under vacuum forming purple oil. After precipitation with 40 mL of CH_2Cl_2, the green solution was dried under vacuum forming a brown powder.

IR (cm^{-1}): 3278 (m.); 2961 (m.); 2930 (m.); 2871 (m.); 1616 (s.); 1573 (m.); 1461 (s.); 1399 (m.); 1369 (w.); 1294 (w.); 1259 (w.); 1204 (w.); 1167 (m.); 1104 (w.); 1167 (m.); 1104 (w.); 1056 (w.); 1026 (m.); 930 (w.); 886 (s.); 847 (w.); 791 (s.); 738 (w.); 671 (m.); 474 (w.); 443 (w.); 418 (w.).

Reaction of PNP-$^{i}Pr_2$ with $VOCl_2(H_2O)_2$

The addition of **1** (171 mg, 0.5 mmol) in THF to a solution of $VOCl_2(H_2O)_2$ (86.9 mg, 0.5 mmol) in the same solvent formed a blue solution. The reaction mixture was stirred for 2 hours, after which the solvent was removed under vacuum, originating a dark brown oil. A brown solid was obtained after precipitation with 40 mL of *n*-Hexane.

IR (cm^{-1}): 3398 (s.); 2979 (vs.); 2872 (s.); 2684 (m.); 1652 (s.); 1461 (s.); 1366 (m.); 1291 (w.); 1243 (w.); 1179 (m.); 1070 (vs.); 998 (m.); 911 (s.); 747 (w.); 723 (w.); 662 (m.); 526 (m.); 503 (m.); 497 (m.); 479 (s.).

Reaction of PNP-$^{i}Pr_2$ with $VOCl_2(H_2O)_2$ and $P(Ph)_3$

This reaction was carried analogously to the latter one. To the blue reaction mixture containing **1** (171 mg, 0.5 mmol) and $VOCl_2(H_2O)_2$ (86.9 mg, 0.5 mmol) in THF, $P(Ph)_3$ (131 mg, 0.5 mmol) was added. After being stirred for 2 hours, the colour of the solution turned to green with a white precipitate that was then filtered off. Crystals suitable for single crystal x-ray diffraction were obtained from the diffusion of Et_2O into a concentrated THF solution.

IR (cm^{-1}): 3406 (vs.); 2436 (m.); 1653 (vs.); 1475 (m.); 1435 (m.); 1391 (w.); 1322 (w.); 1301 (w.); 1173 (m.); 1113 (m.); 1091 (m.); 1066 (m.); 996 (s.); 935 (w.); 901 (w.); 884 (w.); 742 (s.); 696 (s.); 669 (s.); 656 (s.); 632 (s.); 618 (s.); 596 (s.); 573 (s.); 566 (s.); 553 (s.); 527 (s.); 514 (s.); 501 (s.); 471 (s.); 460 (s.); 438 (s.); 433 (s.); 426 (s.); 411 (s.)

APPENDIX

Crystallographic and Experimental Details of Data Collection and Crystal Structure Determinations

Table AP1 - Crystal data and structure refinement for $[V(PNP\text{-}^{i}Pr_2)Cl_3] \cdot CH_2Cl_2$ (3a)

Empirical formula	C18 H35 Cl5 N3 P2 V	
Formula weight	583.62	
Temperature (K)	150(2)	
Wavelength (Å)	0.71073	
Crystal system, space group	Orthorhombic, P2(1)2(1)2(1)	
Unit cell dimensions	a (Å) = 9.881(1)	α (º) = 90
	b (Å) = 15.148(2)	β (º) = 90
	c (Å) = 18.924(2)	γ (º) = 90
Volume ($Å^3$)	2832.5(6)	
Z	4	
Calculated density ($g.cm^{-3}$)	1.369	
Absorption coefficient (mm^{-1})	0.946	
F(000)	1208	
Crystal size (mm)	0.04 x 0.08 x 0.12	
θ range for data collection (º)	2.33 – 25.67	
Limiting indices	$-12 \leq h \leq 7$, $-11 \leq k \leq 18$, $-20 \leq l \leq 23$	
Reflections collected/unique	8012 / 4644 [R_{int} = 0.0549]	
Completeness to θ (%)	99.1	
Absorption correction	Multi-scan	
Refinement method	Full-matrix least-squares on F^2	
Data / restraints / parameters	4644 / 2 / 278	
Goodness-of-fit on F^2	0.969	
Final *R* indices [$I > 2\sigma(I)$]	R_1 = 0.0624, ωR_2 = 0.1501	
R indices (all data)	R_1 = 0.1019, ωR_2 = 0.1696	
Largest diff. peak and hole (eA^{-3})	0.557 and -0.543	

$$R_1 = \frac{\sum \left| |F_0| - |F_c| \right|}{\sum |F_0|} \qquad \omega R_2 = \left[\frac{\sum \omega \left(F_0^2 - F_c^2 \right)^2}{\sum \omega \left(F_0^2 \right)^2} \right]^{\frac{1}{2}}$$

Table AP2 - Crystal data and structure refinement for [V(PNP-^{i}Pr$_2$)Cl$_3$] • THF (3b)

Empirical formula	C21 H41 Cl3 N3 O P2 V
Formula weight	570.80
Temperature (K)	150(2)
Wavelength (Å)	0.71073
Crystal system, space group	Orthorhombic, P2(1)2(1)2(1)
Unit cell dimensions	a (Å) = 11.987(2) α (º) = 90 b (Å) = 12.562(2) β (º) = 90 c (Å) = 37.114(5) γ (º) = 90
Volume (Å^3)	5588.7(15)
Z	8
Calculated density (g.cm^{-3})	1.357
Absorption coefficient (mm^{-1})	0.775
F(000)	2400
Crystal size (mm)	0.08 x 0.080 x 0.10
θ range for data collection (º)	3.19 – 25.35
Limiting indices	$-14 \le h \le 14$, $-15 \le k \le 15$, $-44 \le l \le 44$
Reflections collected/unique	53217 / 10208 [R_{int} = 0.1593]
Completeness to θ (%)	99.7
Absorption correction	Multi-scan
Refinement method	Full-matrix least-squares on F^2
Data / restraints / parameters	10208 / 17 / 591
Goodness-of-fit on F^2	0.992
Final *R* indices [$I > 2\sigma(I)$]	R_1 = 0.0605, ωR_2 = 0.1101
R indices (all data)	R_1 = 0.1107, ωR_2 = 0.1232
Largest diff. peak and hole (eA^{-3})	1.108 and -0.599

$$R_1 = \frac{\sum \left\| F_0 \right| - \left| F_c \right\|}{\sum \left| F_0 \right|} \qquad \omega R_2 = \left[\frac{\sum \omega \left(F_0^2 - F_c^2 \right)^2}{\sum \omega \left(F_0^2 \right)^2} \right]^{\frac{1}{2}}$$

Table AP3 - Crystal data and structure refinement for $[V(PNP\text{-}Ph_2)Cl_3] \cdot (THF)_2$ **(4)**

Empirical formula	C37 H41 Cl3 N3 O2 P2 V	
Formula weight	778.96	
Temperature (K)	150(2)	
Wavelength (Å)	0.71073	
Crystal system, space group	Triclinic, P-1	
Unit cell dimensions	a (Å) = 10.138(1)	α (º) = 92.292(4)
	b (Å) = 10.173(1)	β (º) = 90.705(4)
	c (Å) = 18.543(2)	γ (º) = 101.030(5)
Volume ($Å^3$)	1875.2(3)	
Z	2	
Calculated density ($g.cm^{-3}$)	1.380	
Absorption coefficient (mm^{-1})	0.600	
F(000)	808	
Crystal size (mm)	0.12 x 0.12 x 0.14	
θ range for data collection (º)	2.04 – 27.11	
Limiting indices	$-12 \le h \le 12$, $-11 \le k \le 13$, $-23 \le l \le 22$	
Reflections collected/unique	25016 / 8219 [R_{int} = 0.0600]	
Completeness to θ (%)	99.4	
Absorption correction	Multi-scan	
Refinement method	Full-matrix least-squares on F^2	
Data / restraints / parameters	8219 / 0 / 441	
Goodness-of-fit on F^2	1.050	
Final *R* indices [$I > 2\sigma(I)$]	R_1 = 0.0458, ωR_2 = 0.1117	
R indices (all data)	R_1 = 0.0647, ωR_2 = 0.1203	
Largest diff. peak and hole (eA^{-3})	0.653 and -0.342	

$$R_1 = \frac{\sum \left| |F_0| - |F_c| \right|}{\sum |F_0|} \qquad \omega R_2 = \left[\frac{\sum \omega \left(F_0^2 - F_c^2 \right)^2}{\sum \omega \left(F_0^2 \right)^2} \right]^{\frac{1}{2}}$$

Table AP4 - Crystal data and structure refinement for $[Ti(PNP\text{-}Ph_2)Cl_3] \cdot (THF)_2$ (5)

Empirical formula	C37 H41 Cl3 N3 O2 P2 Ti	
Formula weight	775.89	
Temperature (K)	150(2)	
Wavelength (Å)	0.71073	
Crystal system, space group	Triclinic, P-1	
Unit cell dimensions	a (Å) = 10.090(9)	α (º) = 92.07(4)
	b (Å) = 10.328(9)	β (º) = 90.87(5)
	c (Å) = 18.603(15)	γ (º) = 100.88(4)
Volume ($Å^3$)	1902(3)	
Z	2	
Calculated density ($g.cm^{-3}$)	1.355	
Absorption coefficient (mm^{-1})	0.556	
F(000)	806	
Crystal size (mm)	0.06 x 0.08 x 0.08	
θ range for data collection (º)	1.10 – 25.80	
Limiting indices	$-12 \leq h \leq 12$, $-12 \leq k \leq 12$, $-18 \leq l \leq 22$	
Reflections collected/unique	13005 / 6761 [R_{int} = 0.2241]	
Completeness to θ (%)	92.2	
Absorption correction	Multi-scan	
Refinement method	Full-matrix least-squares on F^2	
Data / restraints / parameters	6761 / 290 / 435	
Goodness-of-fit on F^2	0.856	
Final *R* indices [$I > 2\sigma(I)$]	R_1 = 0.1345, ωR_2 = 0.3216	
R indices (all data)	R_1 = 0.3825, ωR_2 = 0.4238	
Largest diff. peak and hole (eA^{-3})	1.561 and -1.590	

$$R_1 = \frac{\sum \left| |F_0| - |F_c| \right|}{\sum |F_0|} \qquad \omega R_2 = \left[\frac{\sum \omega \left(F_0^2 - F_c^2 \right)^2}{\sum \omega \left(F_0^2 \right)^2} \right]^{\frac{1}{2}}$$

Table AP5 - Crystal data and structure refinement for $[V(PNP^{Me\text{-}i}Pr_2)Cl_3]$ **(7)**

Empirical formula	C19 H37 Cl3 N3 P2 V	
Formula weight	526.8	
Temperature (K)	100(2)	
Wavelength (Å)	0.71073	
Crystal system, space group	Orthorhombic, Pca21	
Unit cell dimensions	a (Å) = 29.6333(3)	α (º) = 90
	b (Å) = 13.8448(3)	β (º) = 90
	c (Å) = 11.9716(7)	γ (º) = 90
Volume ($Å^3$)	4911.6(3)	
Z	8	
Calculated density ($g.cm^{-3}$)	1.4248	
Absorption coefficient (mm^{-1})	0.872	
F(000)	2208	
Crystal size (mm)	0.56 x 0.27 x 0.08	
θ range for data collection (º)	1.37 – 32.68	
Limiting indices	$-44 \le h \le 43$, $-18 \le k \le 21$, $-17 \le l \le 18$	
Absorption correction	Multi-scan	
Refinement method	Full-matrix least-squares on F^2	
Data / restraints / parameters	17420 / 0 / 506	
Goodness-of-fit on F^2	1.76	
Final *R* indices [$I > 2\sigma(I)$]	R_1 = 0.0384, ωR_2 = 0.0421	
R indices (all data)	R_1 = 0.0452, ωR_2 = 0.0430	
Largest diff. peak and hole (eA^{-3})	0.82 and -0.54	

$$R_1 = \frac{\sum \left| |F_0| - |F_c| \right|}{\sum |F_0|} \qquad \omega R_2 = \left[\frac{\sum \omega \left(F_0^2 - F_c^2 \right)^2}{\sum \omega \left(F_0^2 \right)^2} \right]^{\frac{1}{2}}$$

Table AP6 - Crystal data and structure refinement for $[Ag((2,6\text{-}Me)PhNC)_4]PF_6$ **(8)**

Empirical formula	C36 H36 Ag F6 N4 P	
Formula weight	777.53	
Temperature (K)	150(2)	
Wavelength (Å)	0.71073	
Crystal system, space group	Monoclinic, I2/a	
Unit cell dimensions	a (Å) = 22.733(3)	α (º) = 90
	b (Å) = 9.881(1)	β (º) = 92.119(5)
	c (Å) = 15.731(2)	γ (º) = 90
Volume ($Å^3$)	3531.2(7)	
Z	4	
Calculated density ($g.cm^{-3}$)	1.463	
Absorption coefficient (mm^{-1})	0.679	
F(000)	1584	
Crystal size (mm)	0.10 x 0.14 x 0.20	
θ range for data collection (º)	3.05 – 26.44	
Limiting indices	$-27 \le h \le 28$, $-10 \le k \le 12$, $-19 \le l \le 19$	
Reflections collected/unique	15855 / 3626 [R_{int} = 0.0611]	
Completeness to θ (%)	99.5	
Absorption correction	Multi-scan	
Refinement method	Full-matrix least-squares on F^2	
Data / restraints / parameters	3626 / 0 / 223	
Goodness-of-fit on F^2	1.012	
Final *R* indices [$I > 2\sigma(I)$]	R_1 = 0.0358, ωR_2 = 0.0888	
R indices (all data)	R_1 = 0.0486, ωR_2 = 0.0939	
Largest diff. peak and hole (eA^{-3})	0.632 and -0.457	

$$R_1 = \frac{\sum \left| |F_0| - |F_c| \right|}{\sum |F_0|} \qquad \omega R_2 = \left[\frac{\sum \omega \left(F_0^2 - F_c^2 \right)^2}{\sum \omega \left(F_0^2 \right)^2} \right]^{\frac{1}{2}}$$

Table AP7 - Crystal data and structure refinement for $[V(O^tBu)_2(THF)_2(LiCl)_2]$ (9)

Empirical formula	C24 H52 Cl Li2 O6 V	
Formula weight	536.93	
Temperature (K)	150(2)	
Wavelength (Å)	0.71073	
Crystal system, space group	Monoclinic, I2/a	
Unit cell dimensions	a (Å) = 18.681(1)	α (º) = 90
	b (Å) = 9.1090(6)	β (º) = 91.430(4)
	c (Å) = 18.244(1)	γ (º) = 90
Volume ($Å^3$)	3103.5(3)	
Z	4	
Calculated density ($g.cm^{-3}$)	1.149	
Absorption coefficient (mm^{-1})	0.436	
F(000)	1160	
Crystal size (mm)	0.08 x 0.12 x 0.26	
θ range for data collection (º)	3.08 – 27.22	
Limiting indices	$-23 \le h \le 24$, $-11 \le k \le 11$, $-23 \le l \le 23$	
Reflections collected/unique	17556 / 3441 [R_{int} = 0.0715]	
Completeness to θ (%)	99.1	
Absorption correction	Multi-scan	
Refinement method	Full-matrix least-squares on F^2	
Data / restraints / parameters	3441 / 6 / 162	
Goodness-of-fit on F^2	1.077	
Final *R* indices [$I > 2\sigma(I)$]	R_1 = 0.0691, ωR_2 = 0.1736	
R indices (all data)	R_1 = 0.0881, ωR_2 = 0.1849	
Largest diff. peak and hole (eA^{-3})	0.863 and -0.755	

$$R_1 = \frac{\sum \left| |F_0| - |F_c| \right|}{\sum |F_0|} \qquad \omega R_2 = \left[\frac{\sum \omega \left(F_0^2 - F_c^2 \right)^2}{\sum \omega \left(F_0^2 \right)^2} \right]^{\frac{1}{2}}$$

Table AP8 - Crystal data and structure refinement for $[VCl_2(OPPh_3)_2]$ **(10)**

Empirical formula	C36 H30 Cl2 O3 P2 V	
Formula weight	694.38	
Temperature (K)	150(2)	
Wavelength (Å)	0.71073	
Crystal system, space group	Monoclinic, P2(1)/c	
Unit cell dimensions	a (Å) = 16.927(2)	α (º) = 90
	b (Å) = 18.121(2)	β (º) = 98.077(7)
	c (Å) = 11.086(1)	γ (º) = 90
Volume ($Å^3$)	3366.7(6)	
Z	4	
Calculated density ($g.cm^{-3}$)	1.370	
Absorption coefficient (mm^{-1})	0.583	
F(000)	1428	
Crystal size (mm)	0.20 x 0.20 x 0.24	
θ range for data collection (º)	1.22 – 25.48	
Limiting indices	$-20 \leq h \leq 19$, $-21 \leq k \leq 21$, $-13 \leq l \leq 13$	
Reflections collected/unique	27672 / 6207 [R_{int} = 0.0791]	
Completeness to θ (%)	99.3	
Absorption correction	Multi-scan	
Refinement method	Full-matrix least-squares on F^2	
Data / restraints / parameters	6207 / 0 / 397	
Goodness-of-fit on F^2	1.000	
Final *R* indices [$I > 2\sigma(I)$]	R_1 = 0.0434, ωR_2 = 0.0881	
R indices (all data)	R_1 = 0.0848, ωR_2 = 0.0976	
Largest diff. peak and hole (eA^{-3})	0.296 and -0.345	

$$R_1 = \frac{\sum \left| |F_0| - |F_c| \right|}{\sum |F_0|} \qquad \omega R_2 = \left[\frac{\sum \omega \left(F_0^2 - F_c^2 \right)^2}{\sum \omega \left(F_0^2 \right)^2} \right]^{\frac{1}{2}}$$

References

1 King, R.B., *Transition-Metal Organometallic Chemistry An Introduction;* Academic Press, INC 1969.

2 Moulton, C.J.; Shaw B.I., *Dalton Transactions* 1976; 11: 1020-1024.

3 Wanniarachchi, S., *The Impact of Ligand Design on the Coordination Chemistry and Reactivity of metal pincer complexes;* 2009, Marquette University.

4 Benito-Garagorri, D.; Becker, E.; Wiedermann, J.; Lackner, W.; Pollak, M.; Mereiter, K.; Kisala, J.; Kirchner, K., *Organometallics* 2006, 25 (8), 1900-1913.

5 van Koten, G.; Gossage, R.A*., The Privileged Pincer-Metal Plataform: Coordination Chemistry and Applications;* Springer, 2015.

6 Morales-Morales, D.; Jensen, C. M.; *The Chemistry of Pincer Compounds*; Elsevier, Amsterdam, 2007.

7 Morales-Morales, D.; *Pincer complexes. Applications in Catalysis;* Rev. Soc. Quím. Méx. 2004, 48, 338-346.

8 Yoon, M.; Ryu, D.; Kim, J, Ahn, K. H. *Organometallics*, 2006, *25,* 2409–2411.

9 Kozlov, L. A.; Aleksanyan, D. V.; Nelyubina, Y. V.; Lyssenko, K. A.; Petrovskii, P. V.; Vasil'ev, A. A.; Odinets, I. L.*Organometallics*, 2011, *30,* 2920–2932.

10 G Suzuki, A. *J. Organomet. Chem*. 1999, 576, 147–168.

11 Baumann, R.; Davis, W. M.; Schrock, R. R. *J., Am. Chem. Soc.* 1997, *119*, 3830.

12 Naota, T.; Takaya, H.; Murahashi, S.-I.,*Chem. Rev.* 1998, *98*, 2599.

13 Bedford, R. B.; Draper, S. M.; Scully, P. N.; Welch, S. L. *New J., Chem*. 2000, *24*, 745–747.

14 Ohff, M.; Ohff, A.; van der Boom, M. E.; Milstein, D. *J., Am. Chem. Soc.* 1997, *119*, 11687–11688.

15 Liu, F.; Pak, E. B.; Singh, B.; Jensen, C. M.; Goldman, A. S*. J., Am. Chem. Soc*. 1999, *121*, 4086–4087.

16 Longmire, J. M.; Zhang, X., *Tetrahedron Lett*. 1997, *38*, 1725–1728.

17 Schirmer, W.; Flörke, U.; Haupt, H.J.Z.; *Anorg. Allg. Chem*. 1987, 545, 83–97.

18 Garg, J.A.; Chakraborty, S.; Ben-David, Y.; Milstein, D., *Chem. Commun.*, 2016, 52, 5285-5288.

19 Bichler, B.; Holzhacker, C.; Stöger, B.; Puchberger, M.; Veiros, L.F.; Kirchner, K., *Organometallics*, 32, 2013, 10; S. 4114 - 4121.

20 Bichler, B.; Glatz, M.; Stöger, B.; Mereiter, K.; Veiros, L.F.; Kirchner, K.; *Dalton Transactions*, 43, 2014, S. 14517 - 14519.

21 Glatz, M.; Bichler, B.; Mastalir, M.; Stöger, B.; Weil, M.; Mereiter, K.; Pittenauer, E.; Allmaier, G.; Veiros, L.F.; Kirchner, K., *Dalton Transactions*, 44, 2015, S. 281 - 294.

22 Smith, A.D.; Saini, A.; Singer, L.M.; Phadke, N.; Findlater, M.; *Polyhedron* 2016, 0277-5387.

23 Colthup, N.B.; Daly, L.H.; Wiberley E.S., *Introduction to Infrared and Raman Spectroscopy*; Academic Press International Edition, 1964.

24 Evans, D. F.; *J. Chem. Soc*. 1959, 36, 2003.

25 Evans, D. F.; Fazakerley, G. V.; Phillips, R. F., *J. Chem. Soc*. 1971, A, 1931.

26 Evans, D. F.; Jakubovic, D. A., *J. Chem. Soc., Dalton Trans*. 1988, 2927.

27 Grant, D. H., *J. Chem. Educ.* 1995, 72, 39.

28 Chatterjee, M.; Saktiprosad, G., *Transition Met. Chem*, 23, 355-356 (1998).

29 Öztopcu, ö.; Holzhacker, C.; Puchberger, M.; Weil, M.; Mereiter, K.; Veiros, L.F.; Kirchner, K., *Organometallics*, 32, 2013, 15; S. 3042 - 3052.

30 Hirao, T., *Chem. Rev.*, 1997, 97(8).

31 da Silva, J.A.L; Fraústo da Silva, J.J.R.; Pombeiro, A.J.L., *Coordination Chemistry Reviews* 255(2011) 2232-2248.

32 Marui, K.; Higashiura, Y.; Kodama, S.; Hashidate, S.; Nomoto, A.; Yano, S.; Ueshima, M.; Ogawa, A., *Tetrahedron* 70(2014) 2431-2438.

33 Aslam, S.; Isab A.A.; Alotaibi M.A.; Saleem M.; Monim-ul-Mehboob M.; Ahmad S.; Georgieva I.; Trendafilova N., *Polyhedron* 2016, 212-218.

34 Davidson, G., *Spectroscopic Properties of Inorganic and Organometallic Compounds. Volume 29;* The Royal Society of Chemistry, 1996.

35 Barroso, S.D., *Diaminebisphenolate Titanium, Zirconium and Vanadium Complexes: Synthesis, Reactivity and Applications;* 2010, Instituto Superior Técnico, Lisboa.

36 A. W. Addison, T. N. Rao, J. Reedijk, J. van Rijn, G. C. Verschoor, J. Chem. Soc., Dalton Trans. 1984, 1349-1356.

37 C. O'Sullivan, G. Murphy, B. Murphy, B. Hathaway, J. Chem. Soc., Dalton Trans. 1999, 1835-1844.

38 Orpen, A.G.; Brammer, L,; Allen, F.H.; Kennard, O,; Watson, D.G.; Taylor, R., *J. Chem. Soc.*, *Dalton Trans.* 1989, S1-S83.

39 Manzer, L.E. *Inorg. Synth.* 1982, 21, 135.

40 Jones, N.A.; Liddle, S. T.; Wilson, C.; Arnold, P. L. *Organometallics* 2007, 26, 755.

41 den Haan, K.H.; de Boer, J.L.; Teuben, J.H.; Spek, A.L.; Kojic-Prodic, B.; Hays, G.R.; Huis, R. *Organometallics* 1986, 5, 1726.

42 Sheldrick, G.M.; *SADABS*, *Program for Empirical Absortion Corrections;* University of Göttingen: Göttingen, Germany, 1996.

43 Altomare, A.; Cascarano, G.; Giacovazzo C.; Guagliardi, A., *J. Appl.Crystallogr.*, 1993, 26, 343-350.

44 Altomare, A.; Burla, M.C.; Camalli, M.; Cascarano, G.L.; Giacovazzo, C.; Guagliardi, A.; Moliterni, A.G.G.; Polidori, G.; Spagna, R., *J. Appl.Crystallogr.*, 1999, 32, 115.

45 Burla, M.C.; Caliandro, R.; Camalli, M.; Carozzini, B.; Cascarano, G.L.; De Caro, L.; Giacovazzo, C.; Polidori, G.; Spagna, R., *J. Appl.Crystallogr.*, 2005, 38, 381.

46 Sheldick, G.M.; *Acta Crystallographica Section A. Foundations of Crystallography.,* 2008, 64, S112-S122.

47 Farrugia, L.J.; *J. Appl.Crystallogr.*, 1999, 32, 837.

48 Farrugia, L.J.; *J. Appl.Crystallogr.*, 1997, 30, 565.